THESIS

Cosmological Phase Transitions and Evolution of Topological Defects

宇宙論的相転移と位相的欠陥の進化

MICHIYASU NAGASAWA

長 澤 倫 康

(1)

THESIS

Cosmological Phase Transitions and Evolution of Topological Defects

Michiyasu Nagasawa

A dissertation submitted to
Department of Physics,
School of Science,
The University of Tokyo

December, 1993
UTAP-172

Contents

Chapter 1

Introduction

Modern cosmology has been trying to unveil various enigmas concerning our universe. It, however, is the only universe that we can observe. Nor can we create any universe artificially to make useful and ambitious experiments which are indispensable to the understanding of nature. Thus it is impossible for us to compare our universe with those in other evolutionary stages or those born under different initial conditions. The only thing that we can do is to collect the information from the sky passively. It is a rather irritating situation. Nevertheless the universe has an abundance of possibility as an exhibition of high energy physics world. It is widely believed that the universe was once in extremely hot and dense state that cannot be reproduced in laboratories.

In the thesis, one of the outcomes is reported when the particle physics is applied to the early universe. The main subject is the generation and the evolution of topological defects. In the rest of this chapter, basic concepts and terms which will be used hereafter are introduced. In the chapter 2, the dynamics of a quantum phase transition during the inflation is studied. Such a transition is associated with the natural production mechanism of topological defects. The properties of the concrete examples of topological defects, domain walls surrounded by global strings and global textures, are investigated in the chapters 3 and 4 respectively. Finally the chapter 5 is devoted to the conclusion.

Throughout the thesis, we set $c = \hbar = k_{\mathrm{B}} = 1$, that is, we employ the unit where the light velocity, the Planck constant divided by 2π and the Boltzmann constant are normalized to unity.

1.1 The Standard Cosmology

The first successful physical view of the universe is based on the Big Bang model[1, 2]. This model is constructed from general relativity, the most reliable classical gravitational theory and the cosmological principle, the assumption that the universe is globally homogeneous and isotropic. In the scheme of the general relativity, space and time are not given *a priori*. They should be called a spacetime which evolves dynamically. Under the cosmological principle, the universe is described as a Riemannian spacetime manifold whose metric is the Friedmann-Robertson-Walker one :

$$ds^2 = g_{\mu\nu}dx^\mu dx^\nu = dt^2 - a^2(t)\left[\frac{dr^2}{1-kr^2} + r^2\left(d\theta^2 + \sin^2\theta\, d\varphi^2\right)\right], \tag{1.1}$$

$$= a^2(\tau)\left[d\tau^2 - \frac{dr^2}{1-kr^2} + r^2\left(d\theta^2 + \sin^2\theta\, d\varphi^2\right)\right], \tag{1.2}$$

where τ is the conformal time which is defined by $d\tau = dt/a(t)$. This metric leaves two degrees of freedom. One is the sign of the spatial curvature, k, which represents whether the universe is closed, flat or open depending on $k = 1$, 0 or -1. The other is the scale-factor, a, which describes the time evolution of the size of the universe. The dynamics of the scale-factor is determined by the Einstein equation. In favor of the cosmological principle, the form of the energy-momentum tensor is written by that of the perfect fluid :

$$T^\mu_{\ \nu} = \mathrm{diag}\,(-\rho, p, p, p)\ , \tag{1.3}$$

where ρ is the energy density of the universe and p is the pressure. Both of them depend only on the time not on the spatial coordinates. As a result, the behavior of a, ρ and p are determined by two independent Einstein equations :

$$\left(\frac{\dot{a}}{a}\right)^2 + \frac{k}{a^2} = \frac{8\pi G}{3}\rho + \frac{\Lambda}{3}\ , \tag{1.4}$$

$$\frac{d}{da}\left(\rho a^3\right) + 3pa^2 = 0\ , \tag{1.5}$$

and the equation of state for the ingredients that fill the universe :

$$p = p(\rho)\ . \tag{1.6}$$

In the equation (1.4), the dot denotes the derivative by t; G is the gravitational constant; and Λ is the cosmological constant, which is the energy density of vacuum..

According to the conventional classification, the components of our universe are divided to the non-relativistic dust matter and the radiation. They obey the equations of state :

$$p(\rho) = \begin{cases} 0 & \text{Matter}\ , \\ \dfrac{\rho}{3} & \text{Radiation}\ . \end{cases} \tag{1.7}$$

Hence the energy density of the matter, ρ_m, and that of the radiation, ρ_r, are related to the scale-factor as

$$\rho_m = \rho_{m0}\left(\frac{a_0}{a}\right)^3, \tag{1.8}$$

$$\rho_r = \rho_{r0}\left(\frac{a_0}{a}\right)^4, \tag{1.9}$$

where a_0 is the scale-factor at present, and ρ_{m0} and ρ_{r0} are ρ_m and ρ_r at $a = a_0$. Thus with a decrease in the scale-factor, the energy density increases. At the very early stage, the universe must have experienced an extreme high energy state, which is the so-called Big Bang.

There are three pieces of observational evidence for the Big Bang; the fact that our universe is expanding, that is, the Hubble law; the cosmic microwave background radiation(CMBR) which is the relic of the era when the universe was once in the thermal equilibrium; and the amount of the light elements in the universe. In addition the very small anisotropy of the CMBR on various scales[3] confirms the cosmological principle. Moreover the cosmic background explorer(COBE) has recently detected finite amplitude of fluctuations[4] in the CMBR:

$$\frac{\delta T}{T} = 1.1 \pm 0.2 \times 10^{-5}\ , \quad \text{at angular separation} = 10^\circ\ , \tag{1.10}$$

$$\frac{Q_T}{T} = 5 \times 10^{-6}\ , \quad \text{quadrupole moment}\ . \tag{1.11}$$

This is the definite evidence for the fact that the universe is not perfectly homogeneous at the time of the last scattering.

The standard Big Bang model is impressively successful. However, it contains some serious difficulties which cannot be solved without any resort to other paradigms. Now we show some examples of the faults. Various observations tell us that the universe is almost flat. Besides the cosmological constant is comparable with or much smaller than the ordinary matter energy density. This is unnatural since the terms in the equation (1.4) have

so different dependence on time that in the very first stage of the Big Bang their magnitudes should have been balanced with an extreme fine tuning in order to be consistent with the present observations. These are the flatness problem and the cosmological constant problem.

Next we introduce the horizon problem. The equation (1.10) says that the temperature of the CMBR is very isotropic. This means that the universe was homogeneous at least in the scale that would grow into the particle horizon today. On the other hand, the horizon scale when the radiation and matter at the last scattering corresponds to $\theta \sim 3°$. Thus we have to conclude that the light rays that were emitted from causally separated regions at that era have the identical temperature.

Moreover, the cosmological structures such as stars, galaxies, clusters of galaxies and superclusters should evolve from the primordial fluctuations whose origin is unaccountable in the standard Big Bang model. Since the CMBR is the redshifted photons that were in the thermal equilibrium with matter, the isotropy of the CMBR puts a stringent constraint on the amplitude of fluctuations in matter. This is one of the most fundamental and important problems in the cosmology. In the chapter 3, the possibility of the structure formation by global textures is referred.

There are some other difficulties in addition to ones we have stated above though we do not mention them anymore here. In the most innocent and indifferent view, the responsibility can be taken by the initial state of the universe; we should regard the universe was born as it was anyway. It can be resorted to the anthropologic principle[5] in part. Here we, however, stand the point that the problems which the standard cosmology could not solve can be explained in the frame of the inflationary cosmology[6, 7, 8], which is briefly introduced in the next section. The reasons are that the potential theoretical development seems to be the richest and with this model people probably content their esthetics, which is often essential to the construction of the first principle.

Of course, these problems are rather philosophical ones. In fact, there is a practical problem in the standard cosmology we must confront seriously. There is no final answer of the set of the cosmological parameters which satisfies all the currently available observations[2, 9]; the age of the universe[10], the total amount of mass in the universe[9], the rate of the expansion of the universe[11], so on. Some people still believe the steady state universe[12] instead of the Big Bang model. Although we have to be careful in deciding which is right,

we employ the conventional point of view, the universe has evolved from the hot fireball throughout the present thesis.

Before we close this section, we present some useful formulas. In the chapter 3 and 4, we set $\Lambda = 0$ for simplicity. Under this assumption the parameters which determines the properties of the universe are the Hubble parameter, H, and the density parameter, Ω :

$$H(t) \equiv \frac{\dot{a}(t)}{a(t)}, \tag{1.12}$$

$$\Omega(t) \equiv \frac{\rho(t)}{\rho_{cr}(t)}, \quad \rho_{cr}(t) \equiv \frac{3H^2(t)}{8\pi G}. \tag{1.13}$$

When $\rho >(<) \rho_{cr}$, the universe is close(open) and in the flat universe $\Omega = 1$. At the equality time, *i.e.*, when ρ_m is equal to ρ_r the scale-factor is given by

$$\frac{a_{eq}}{a_0} = 4 \times 10^{-5}(\Omega_0 h^2)^{-1}, \tag{1.14}$$

where Ω_0 is the present value of Ω and h is the Hubble constant in units of 100 km s^{-1}Mpc^{-1}. The observational estimates of these parameters range[9, 11] :

$$0.1 \lesssim \Omega_0 \lesssim 1, \tag{1.15}$$

$$0.4 \lesssim h \lesssim 1.1. \tag{1.16}$$

The above uncertainty is rather unsatisfactory. However, even if the parameters in the standard picture are not determined, it is a valuable trial to develop more refined framework of cosmology since it may fortunately predict the values of such parameters theoretically. Actually the flatness of the universe is demanded in the inflation scheme.

1.2 The Inflationary Cosmology

The union of the high energy physics and the cosmology has brought many interesting ideas. One of them is the inflation[8], which has opened a new paradigm in the physical study of the early universe. Its main idea is the domination of the universe by positive vacuum energy. Then the universe expands exponentially and then it is reheated with the released vacuum energy. When this vacuum energy density equals ρ_v, then the scale-factor evolves as

$$a(t) \propto e^{Ht}, \quad H = \left(\frac{8\pi G \rho_v}{3}\right)^{\frac{1}{2}}, \tag{1.17}$$

where the curvature term is neglected. Such a flat cosmological constant dominant universe without matter is called a de Sitter universe. If this rapid expansion lasts long enough, the curvature radius of the universe increase also exponentially so that the flatness problem should be solved. Moreover, since the causally connected region also expands exponentially we do not have to suffer from the horizon problem. Although there is a doubt whether an initially inhomogeneous or anisotropic universe, which is quite natural, could be inflated to a homogeneous and isotropic one, the generality of the inflation is plausible since the cosmic no hair conjecture[13] seems to be widely applicable.. In fact, the universe after the inflation should not be strictly homogeneous due to the extended quantum fluctuations. These inhomogeneity can provide the initial seeds for the cosmological structure formation. Thus after the reheating, the universe undergoes the standard Big Bang history without serious difficulties in the standard picture.

The origin of the vacuum energy which is necessary for the inflation differs depending on various models. The scalar field which is the source of this zero-point energy is called a inflaton. The first inflation model is proposed from the first-order phase transition in the grand unified theory(GUT) of the elementary interactions[6, 7]. In such a transition, ρ_v is supplied by the false vacuum energy of the Higgs field which is left in the symmetric state during the over-cooling of the universe. This model, however, possesses an important fault, the eternal inflation[6, 14]. The termination of the phase transition should occur through the percolation of the true vacuum bubbles. However, the volume where the inflaton, that is, the Higgs field is in the false vacuum state increases continuously so that the universe inflates for ever. The original inflation model have some other additional difficulties. For example, there should be too much inhomogeneities by the formation of black holes and worm holes[14] and magnetic monopoles should be overproduced[15].

Hence a lot of alternatives have been considered until now. The new inflation model[16] gains the vacuum energy from the Coleman-Weinberg type potential in the SU(5) GUT[17]. In this model, the exponential evolution is realized while the inflaton is rolling down along the gentle slope of the potential slowly. Although the new inflation model does not suffer from the problems which the original model has, there exist other difficulties such as the lack of the inflationary era[16] and the excessive amplitude of the density fluctuations[18].

The extended inflation model[19] is one of the power-law inflation models. It does not

cause the exponential expansion but the power of the scale-factor to time is large enough to solve the horizon or flatness problem. This model consists of the old inflation model plus the Jordan-Brans-Dicke gravitational theory[1]. However, the experimental limit against the time variation of the gravitational parameter is incompatible with the constraint to the remaining density fluctuations predicted in the model[20].

Besides these two models, there are many versions of the inflation in which the inflaton potential is deformed and/or the non-Einstein gravitational theory is included[21]. Nevertheless, we do not have the definite model of the inflation which is consistent with all the existing observations and physical theories. Although the inflationary model has lost a part of appealing features, it is definitely the most fascinating idea to improve the Big Bang model.

Among diverse models the most natural and successful one so far is the chaotic inflation model[22]. This model is unrelated to the phase transition. The vacuum energy, ρ_v is earned by the displacement of the inflaton field from the potential minimum. Such a condition is realized by the quantum fluctuations in the Planck era due to the uncertainty principle. In order to remove the difficulties in the standard model, the potential gradient should be shallow enough for the universe to expand rapidly. Although the observational constraint to the density fluctuations demands that the model parameter should be a very small number[23], the chaotic inflation model has no essential difficulty. It can be also generalized by the non-Einstein gravity theories[24]. The realistic model of the inflaton certainly exists; sneutrino in the super-symmetry(SUSY) model is one of the candidates[25]. In addition, the idea that the universe starts with the very chaotic state is quite natural. Thus we employ the chaotic inflation model in the next chapter.

1.3 Topological Defects

Topological defects are peculiar structures in the spacetime[26, 27]. They are created when the phase transitions accompanied by some kinds of spontaneous symmetry breakings(SSB) occur. SSB is a fairly common phenomena in the unified theory of elementary particle physics. Such a recovery of the today broken symmetry is believed to be achieved in the

very early universe. For example, consider a real scalar field with the Lagrangian :

$$\mathcal{L} = \frac{1}{2}(\partial_\mu \chi)^2 - V(\chi), \qquad M_\chi^2 \equiv \left.\frac{d^2V}{d\chi^2}\right|_{\chi=0} . \tag{1.18}$$

When the effective mass, M_χ^2, turns from positive to negative, the ground states of the potential change.

	Ground State	Symmetry Group
$M_\chi^2 > 0$:	$\chi = 0$	G
$M_\chi^2 < 0$:	$\chi = \pm v \ \left(\propto \sqrt{\lvert M_\chi^2 \rvert}\right)$	H

The Lagrangian itself is symmetric under the reflective transformation of χ. On the other hand, χ settles in $+v$ or $-v$, which is a symmetry broken state. At the phase transition from the higher symmetric vacuum to the lower symmetric vacuum the value of χ becomes inhomogeneous at each domain in the universe. Then the false vacuum energy is preserved in the boundaries between different vacuum states. These left-behind symmetric vacuum structures are called topological defects. They are stable since the defect disposition cannot be erased through continuous variation of χ. An exception is a texture which is an unstable topological defect. What kind of defects will be formed depends on the structure of the true vacuum manifold, M=G/H.

When the discrete symmetry breaks spontaneously, a domain wall, a plain-like defect is produced. In general, $\Pi_0(\mathrm{M}) \neq \mathbf{1}$ is the condition of domain wall production. When the potential is

$$V(\chi) = \frac{1}{4}\lambda(\chi^2 - v^2)^2 , \qquad \chi : \text{real scalar field} , \tag{1.19}$$

the field equation is reduced to

$$\Box\chi + \lambda\chi(\chi^2 - v^2) = 0 . \tag{1.20}$$

Then the field configuration which expresses one static infinite domain wall in xy-plane is

$$\chi(z) = v\tanh\left(\frac{z}{\delta_w}\right) , \qquad \delta_w \equiv \left(\frac{\lambda}{2}\right)^{-\frac{1}{2}} v^{-1} , \tag{1.21}$$

where δ_w is the characteristic length of the wall corresponding to a wall thickness. Since the false vacuum energy equals λv^4, the surface energy density of the wall, σ, is

$$\sigma \sim \lambda v^4 \cdot \delta_w \sim \lambda^{\frac{1}{2}} v^3 . \tag{1.22}$$

However, if only one horizon-size wall exists, the ratio of the energy density of the wall to the critical energy density, Ω_w :

$$\Omega_w \sim 10^{10}\lambda^{\frac{1}{2}}\left(\frac{v}{100\ \mathrm{GeV}}\right)^3 \tag{1.23}$$

exceeds overwhelmingly one when v is approximately given by the GUT energy scale. The anisotropy of CMBR should also become too large[28]. Hence the wall producing phase transition cannot happen at the natural unification scale. Domain walls must be formed at the very late time in the cosmic history. Such a phase transition after the decoupling of matter and photon may be responsible for the large-scale structure formation[29].

When $\Pi_1(\mathrm{M}) \neq \mathbf{1}$ a cosmic string is generated. For example, a complex scalar field, χ, obeying the potential :

$$V(\chi) = \frac{1}{4}\lambda(|\chi|^2 - v^2)^2 , \qquad \chi : \text{complex scalar field} , \tag{1.24}$$

enables the string formation since $\mathrm{M}=\mathrm{S}^1$. If the value of the phase of χ changes after the travel around a closed curve, then at somewhere inside the curve there should be a singular place where the phase cannot be a smooth function. This line-like defect is a string. The phase change around a string must be $2\pi n$, where n is an integer called winding number. Even when M is simply connected, a stable string solution is possible[30]. It can be applied to the electroweak phase transition[31]. When the broken symmetry is global, strings are called global strings. On the other hand, when the gauged symmetry concerns, they are called local or gauged strings. In both cases, the characteristic length that corresponds to the core radius of a string, δ_s, is expressed by the Compton wavelength of χ :

$$\delta_s \sim M_\chi^{-1} \sim \lambda^{-\frac{1}{2}} v^{-1} , \tag{1.25}$$

which is similar to the equation (1.21). The line energy density of a string, μ, is

$$\mu \sim \lambda v^4 \cdot \delta_s^2 \sim v^2 . \tag{1.26}$$

Cosmic strings are considered to produce scale-invariant density perturbations. If the initial seeds for the cosmological structures are given by strings, the symmetry breaking scale should be

$$v \sim 10^{16}\ \mathrm{GeV} , \tag{1.27}$$

which is in the range of the grand unification scale. The detailed mechanism depends on how strings evolve and numerical simulations have been used in order to investigate it[32]. Roughly speaking collapsing string loops or wakes of long strings attract matter and the self-gravitational instability follows[9]. The observational constraints on the existence of strings can be obtained by gravitational waves[33] or radiated particles[34] from collapsing loops, lensing effects of strings[35], CMBR distortion[36], black hole formation[37] and others. Although some of them might exclude the possibility of the structure formation scenario by cosmic strings, parameters in the theory has not been perfectly determined so far. We have to be cautious in concluding there is a reliable observation that contradicts the value of the equation (1.27).

At a phase transition whose $\Pi_2(\mathrm{M}) \neq \mathbf{1}$, a monopole configuration is attained. It is also classified to a global monopole and a local or gauged monopole similar to the string case. The formation of magnetic monopoles is expected in almost all grand unified theories including the electro-magnetic interaction[27, 38]. Thus the detection of magnetic monopoles is an important clue to verify unified theories. However, the mass of them, m_m, is estimated as

$$m_m \sim \frac{2\pi v}{g} \sim 10^{16}\ \mathrm{GeV}\ , \tag{1.28}$$

where v is the symmetry breaking energy scale and g is the gauge coupling constant[39]. If the number density of monopoles is the same order as that of nucleons, they should be catastrophic to the standard evolution of the universe. This is the so-called monopole problem. This another trouble in the standard Big Bang model will be solved by the inflation model in which dilutes the number density of monopoles.

A texture comes into existence when the SSB in which a vacuum manifold has a non-shrinkable three-sphere, that is, $\Pi_3(M) \neq \mathbf{1}$ is realized. In the texture configuration, there is no remnant false vacuum where the symmetric state is left. For this reason, the energy of textures would be canceled if a gauge field participates in the model. Thus a term, a local texture is nonsense. There exists only a global texture. Global textures can provide density fluctuations for the cosmological structure formation[40, 41, 42, 43], which will be described in the chapter 4 more extensively.

Moreover, multiple phase transitions give birth to complex topological defects. For instance, when two scales of transitions symbolized by

$$\mathrm{G} \xrightarrow{1} \mathrm{H} \times \mathrm{U}(1) \xrightarrow{2} \mathrm{H}$$

are accomplished, pairs of a monopole and an anti-monopole connected by strings are formed[44]. Another example, a wall surrounded by a string[45] is investigated in the chapter 3 with relation to an axion model[46]. Such a defect is produced by a symmetry breaking :

$$\mathrm{G} \xrightarrow{1} \mathrm{H} \times \mathbf{Z}_2 \xrightarrow{2} \mathrm{H}\ .$$

From what has been stated above, we can see that in the cosmological context topological defects are noticeable from two distinct aspects: how to get rid of them without destroying the successful description of the standard cosmology and the possibility of the solution for the initial density fluctuation problem in the universe.

1.4 Relations between Cosmological Observations and Particle Physics

The application of the particle physics theory to the early universe brings numerous observational predictions. One of them by the inflation is that $\Omega_0 = 1$ if $\Lambda = 0$. Various observations have been made but the value of the density parameter ranges broadly as in the equation (1.15). They claim that the value close to the flat universe is unprobable so that the cosmological constant should be finite in order to make the inflationary model survive. Part of observations including the age of the universe[10] suggest the existence of Λ[47]. This fact casts another fine tuning problem to the cosmology, which is strongly linked with the extreme high energy scale physics. Some people refer to a decaying cosmological constant[48], which cannot be a final answer to the question since the drastic energy liberation of it should have happened someday during the cosmic past life. Anyway when we investigate the cosmological evolution, a flat model with or without the cosmological constant and an open model is generally adopted.

From the calculation of the light elements abundance by primordial nucleosynthesis the constraint on the cosmological parameters is gained[2, 49] :

$$\Omega_b h^2 \lesssim 0.02\ , \tag{1.29}$$

where Ω_b is the portion of the baryon contribution to Ω_0. Baryonic matter corresponds to only a part of the energy density in the universe in the equation (1.15) Thus the existence of non-baryonic dark matter is necessary. Although the identification of dark matter is still obscure, there are numerous candidates in particle physics models[2]. Non-baryonic dark matter is roughly classified to cold dark matter(CDM) and hot dark matter(HDM). CDM is named after the property that it is non-relativistic at the getting out from the thermal equilibrium. Axions or some SUSY particles are examples of CDM. On the other hand, HDM is called hot since it was relativistic at the time of running out from the equilibrium. Massive neutrino belongs to this class of dark matter.

Using the above arguments scenarios for the large-scale structure formation in the universe can be constructed. There are many versions including various cosmological parameters, different type of ingredients but most of them are based on the clustering of matter by the gravitational instability and the initial seeds for mass accretion are supplied by particle physics; inflation and/or topological defects. Both of them provide the primordial density perturbations of scale-invariant power spectrum.

In the inflationary era, quantum fluctuations are extended to those on classical scales, which have cosmological importance[18, 23, 50]. The scales of fluctuations spread over the Hubble length, H^{-1}. Thus various scales of fluctuations appear. After the end of the inflation, the universe is filled with the ordinary matter and the Hubble length evolves as $H^{-1} \propto a^2(t)$ in the radiation dominated era and $H^{-1} \propto a^{\frac{3}{2}}(t)$ in the matter dominated era. On the other hand, the fluctuations which go beyond the Hubble length during the inflationary expansion grow in proportion to the scale-factor. As a result, over-horizon fluctuations again enter into the region where we can observe. In these processes, fluctuations of the power spectrum :

$$\left\langle \left| \frac{\delta\rho}{\rho} \right|_k^2 \right\rangle \propto k \,, \tag{1.30}$$

i.e., the Harrison-Zel'dovich spectrum[51] are obtained. Their amplitude is identical at the horizon crossing epoch. Such mechanisms create scale-invariant density perturbations for the structure formation in the universe.

In many aspects particle theory compensates for the shortcomings of the Big Bang model. Such considerations associate astronomical observations with physics in very high energy scales. In particular, the observations of the cosmological structures are immensely valuable. One of the observations which reveal the properties of the density perturbations in the universe is acquired by the direct investigation of the matter, that is, galaxy distribution. Another important observation is the CMBR anisotropy in the equation (1.10). Hence the scenario must explain these two observations without any contradiction. Theoretically, detailed properties of various scenarios are elucidated by numerical simulations[52]. However, even the most standard one, in which the flat universe, CDM, and the Gaussian scale-invariant initial fluctuations are assumed is perfectly satisfactory[53]. Roughly speaking it is difficult to reconcile the amazing smallness of CMBR anisotropy with the wide variety of the way of galaxy distribution[54].

The very large-scale structure such as voids[55], the Great Wall[56], periodic structure[57] imply intensive correlations of matter on scales $\gtrsim 100$ Mpc. Observationally, it can be said that galaxies are distributed in a highly non-Gaussian manner[58]. It might have resulted from the non-Gaussian initial fluctuations. Furthermore, the suppression of the CMBR anisotropy can be attained by a possible reionization of the universe[59]. Such process occurs, for instance, by the reheating due to the early star formation. Non-Gaussian initial fluctuations might also have been necessary for the prompt matter collapse. Most of the inflationary model predict the Gaussian density perturbations[23, 50, 60]. There are attempts to produce non-Gaussian peaks by the inflation[61] but most of such renovation request a complicated model so that the generality and naturality, the advantages of the inflation are lost. Even in the case that the inflaton is combined non-linearly with matter fields, averaging effect should smooth out prominent density peaks[62]. On the other hand, topological defects generate non-Gaussian seeds inevitably and they may cause non-gravitational clustering of matter by string wakes[63] or texture knot collapses[40]. The progress of the CMBR observation will make the statistical property of the temperature fluctuations clear and determine which initial model of density perturbations is appropriate[64]. Thus SSB, an indispensable concept to the modern particle physics theory also has strong association with cosmology.

Chapter 2

Creation of Topological Defects

In this chapter, the dynamics of a second-order phase transition during the inflation, which is induced by time-variation of space-time curvature, is studied as a natural mechanism to produce topological defects of typical grand unification scales such as cosmic strings or global textures. It is shown that their energy distribution is almost scale-invariant with small- and large-scale cutoffs. Also discussed is how these cutoffs are given.

2.1 Kibble Mechanism and its Problem

Many people applied unification theories of elementary interactions to the early universe whose temperature, according to the conventional Big Bang cosmology, was once so high as the unification energy scale. One of their natural consequences is that the universe has presumably undergone a number of thermal phase transitions in the course of its early evolution, in some of which topological defects may have been produced through the so-called Kibble mechanism[26].

In this mechanism, at ultra-high temperatures presently broken symmetries are restored due to high-temperature correction to the potential of the Higgs fields which determines the symmetry of the system. The standard Big Bang cosmology enables such a high-energy-density condition in the early universe. For example, a real scalar field, χ, obeying the Lagrangian :

$$\mathcal{L} = \frac{1}{2}(D_\mu\chi)^2 - \frac{1}{4}F_{\mu\nu}F^{\mu\nu} - V(\chi) , \quad V(\chi) = \frac{\lambda}{4}(\chi^2 - v^2)^2 , \tag{2.1}$$

$$D_\mu = \partial_\mu - igA_\mu , \quad F_{\mu\nu} = \partial_\mu A_\nu - \partial_\nu A_\mu ,$$

acquires the correction term[65] :

$$V_T(\chi) = V(\chi) - \frac{\pi^2}{90}\mathcal{N}(T)T^4 + B(\chi)T^2 + \mathcal{O}(T^1) , \tag{2.2}$$
$$B(\chi) = \frac{\lambda}{12}(\chi^2 - v^2) + \frac{\lambda}{12}\chi^2 + \frac{1}{4}g^2\chi^2 ,$$

where $\mathcal{N}(T)$ is the sum of freedom for all particle species. It can be estimated to be $\mathcal{N}(T) \sim \mathcal{O}(100)$ at the energy scale of $T \sim 10^{15}$ GeV. Then the critical temperature for the phase transition is

$$T_c = \sqrt{\frac{6\lambda}{2\lambda + 3g^2}}v . \tag{2.3}$$

In the course of cosmic evolution, symmetries have been broken and various types of phase transitions should have been actualized. If cosmic strings or global textures may help large-scale structure formation, their energy scale of phase transitions should be around $10^{15\sim16}$GeV[66, 40].

At such a thermal phase transition, the correlation distance of the fluctuations for χ should be similar to the horizon length. Thus the number density of produced topological defects can be estimated to be the order of one defect per horizon scale.

In discussing these phase transitions, it has been implicitly assumed that the universe was in thermal equilibrium state at least by the GUT era. However, in order to attain thermal equilibrium from an arbitrary initial state of the universe, it is necessary that particle interaction rates, Γ, exceed the cosmic expansion rate, H, which is not always possible in such an early stage of cosmic evolution[67]. To see this explicitly, we demonstrate a simple comparison of Γ and H. When χ can be regarded as relativistic particles, its number density, n_χ, is

$$n_\chi \sim \frac{N_\chi}{\pi^2}T^3 , \tag{2.4}$$

where N_χ is the number of modes that are interacting with χ. The scattering cross section of χ, σ_χ, is

$$\sigma_\chi \sim \frac{\alpha_\chi^2}{T^2} , \tag{2.5}$$

where α_χ is a coupling strength. Using above formulas, the reaction rate of χ, Γ, is written by

$$\Gamma = n_\chi\sigma_\chi \sim \frac{N_\chi}{\pi^2}\alpha_\chi^2 T . \tag{2.6}$$

On the other hand, the Hubble parameter is expressed as

$$H = \left(\frac{8\pi^3 G\mathcal{N}}{90}T^4\right)^{\frac{1}{2}} . \tag{2.7}$$

Thus for the condition $\Gamma \gg H$ to hold, it is necessary that

$$T \ll T_{th} \equiv 3 \times 10^{14}\left(\frac{\alpha_X}{0.02}\right)^2\left(\frac{N_X}{10}\right)\left(\frac{\mathcal{N}}{200}\right)^{-\frac{1}{2}} \text{ GeV} . \tag{2.8}$$

Hence the formation of topological defects with typical GUT scale may not be described by the Kibble mechanism correctly unless the universe started its evolution in a thermal equilibrium state.

It is more natural to expect that our universe started its classical evolution out of a chaotic state governed by quantum and thermal fluctuations[22] and that it underwent inflation to be globally homogeneous and isotropic as observed today[7]. Then it turns out that after the reheating epoch the universe was first filled with radiation in thermal equilibrium. Unfortunately, the maximum temperature it experienced, or the reheating temperature, may not be so high as the GUT scale generally in order to avoid too much gravitational waves or density fluctuations[68] and/or too many gravitinos[69] to be produced after the inflation. On the other hand, models with high enough reheating temperature may not solve the monopole problem, even if they may keep large enough density of strings or textures. Thus it is very difficult to obtain a sensible scenario of the early universe which provides an appropriate initial condition of galaxy formation through topological defects in the grand unification scale.

In order to resolve this difficulty several mechanisms of non-thermal phase transitions have been proposed in which the Higgs field is coupled either with spacetime curvature $\mathcal{R}$[70], the inflaton field ϕ[71, 72] or both of them[73]. The first mechanism is especially plausible since the effective potential naturally has a finite-curvature correction in the inflating spacetime just as it would have a finite-temperature correction in the hot Big Bang universe[74]. In these scenarios phase transition takes place during the inflationary stage due to time variation of $\mathcal{R}$ or ϕ and it is triggered by quantum fluctuations rather than thermal fluctuations.

While the properties of thermal phase transitions have been extensively studied, those of the above non-thermal phase transitions have not been fully investigated. The purpose of the

rest of this chapter is to clarify the dynamics of a second-order phase transition during the inflation as well as the spectrum of the defects produced. Complementary to our work[75], Linde and Lyth have studied formation of axionic domain walls through quantum fluctuations during the inflation[76]. The case where topological defects are produced through a first-order phase transition has been considered by Copeland, Kolb, and Liddle[77] in the context of the extended inflation scenario. In addition, quantum creation of defects through tunneling during the inflation has been investigated by Basu, Guth, and Vilenkin[78].

2.2 Quantum Phase Transition during the Inflation

In this section, the model we consider in this chapter is introduced. The metric is that in the spatially flat Friedmann-Robertson-Walker spacetime, *i.e.*, the case of $k = 0$ in the equation (1.1) :

$$ds^2 = dt^2 - a^2(t)d\mathbf{x}^2 = a^2(\tau)(d\tau^2 - d\mathbf{x}^2) . \tag{2.9}$$

As the inflationary model the chaotic inflation scenario realized by a massive scalar field ϕ with mass m is chosen. Hence the inflaton potential is

$$V_I(\phi) = \frac{1}{2}m^2\phi^2 . \tag{2.10}$$

In order for the density fluctuations to be small enough on this scale, m should satisfy the constraint $m \lesssim 10^{13}$GeV[79, 80]. In the inflationary stage when the energy density of the universe is dominated by $V_I(\phi)$, the classical evolution of $\phi(t)$, the scale-factor $a(t)$, and the Hubble parameter $H(t)$, is given by

$$\phi(t) = \phi_i - \frac{mM_{pl}}{2\sqrt{3\pi}}(t - t_i) , \tag{2.11}$$

$$H(t) = \sqrt{\frac{4\pi m^2}{3M_{pl}^2}\phi(t)} = H_i - \frac{m^2}{3}(t - t_i) , \tag{2.12}$$

$$a(t) = a_i \exp\left[\frac{2\pi}{M_{pl}^2}(\phi_i^2 - \phi^2(t))\right] = a_i \exp\left[\frac{3}{2m^2}\left(H_i^2 - H^2(t)\right)\right] , \tag{2.13}$$

respectively, where $M_{pl} \equiv \sqrt{\hbar c/G}$ is the Planck mass and t_i is an arbitrary epoch when $a = a_i$, $\phi = \phi_i$ and $H = H_i$. The above expression is a good approximation when ϕ satisfies the following inequality :

$$\phi_l \equiv \frac{M_{pl}}{\sqrt{4\pi}} \lesssim \phi(t) \lesssim \left(\frac{3}{32\pi}\right)^{\frac{1}{4}}\left(\frac{M_{pl}}{m}\right)^{\frac{1}{4}} M_{pl} \equiv \phi_u . \tag{2.14}$$

For $\phi > \phi_u$ the evolution of ϕ is dominated by quantum fluctuations[81] and at $\phi = \phi_l$ the time variation rate of ϕ or $\dot{\phi}/\phi$ becomes as large as the expansion rate H so that inflationary expansion terminates. The present horizon scale left the Hubble radius when $\phi \approx 3M_{pl}$ corresponding to the e-folding number of inflation after this epoch to be about ≈ 60, which is sufficient for solving the flatness problem and the horizon problem.

As is seen in (2.12), for $H(t) \gtrsim m/\sqrt{3}$ or $\phi \gtrsim M_{pl}/\sqrt{4\pi}$ time variation rate of the Hubble parameter is so small that the evolution of the scale-factor is indistinguishable from that in de Sitter spacetime during each span of several expansion times. Hence we may utilize various results of quantum field theory in de Sitter spacetime.

In the inflationary stage the scalar curvature $\mathcal{R}$ is given by

$$\mathcal{R} = 12H^2 + 6\dot{H} \cong \frac{16\pi}{M_{pl}^2} m^2\phi^2 - 2m^2 \ . \tag{2.15}$$

And we consider the evolution of a scalar field χ with the Lagrangian :

$$\mathcal{L}_\chi = \frac{1}{2}(\partial\chi)^2 - V(\chi) \ , \qquad V(\chi) = \frac{\lambda}{4}(\chi^2 - v^2)^2 + \frac{1}{2}\xi\mathcal{R}\chi^2 \ , \tag{2.16}$$

with a positive coupling parameter ξ to the scalar curvature $\mathcal{R}$.

The effective mass for χ is written as

$$\begin{aligned} M_\chi^2 &= -\lambda v^2 + \xi\mathcal{R} \\ &= -\lambda v^2 + 12\xi H^2(t) - 2\xi m^2 \ . \end{aligned} \tag{2.17}$$

In proportion as the inflaton field rolls down to the potential minimum, the Hubble parameter decreases. Then the symmetry of χ is restored if $\xi\mathcal{R} > \lambda v^2$ and a second-order phase transition takes place as $\mathcal{R}$ decreases gradually. For the symmetry restoration to occur, the condition $M_\chi^2 > 0$ must hold at least when $t = t_i$. It means :

$$\phi_i \ > \ \frac{M_{pl}}{\sqrt{8\pi}}\sqrt{1 + \frac{1}{2\xi}\frac{\lambda v^2}{m^2}} \ . \tag{2.18}$$

Depending on the number of components of χ, j, this system allows a domain wall ($j = 1$), a string ($j = 2$), a monopole ($j = 3$), or a texture ($j = 4$) solution if $\xi\mathcal{R} \ll \lambda v^2$. In discussing the phase transition, however, we concentrate on the single-component case, a real scalar field. Generalization to multi-components cases will be discussed in the final section.

In the case of the quantum phase transition during the inflation, various scales of fluctuations even beyond the Hubble horizon scale are produced. Thus the distribution of topological defects and the mean distance between them are quite different from those in the thermal phase transitions. These properties should be known by considering how the fluctuations of χ behave and what value it takes at each place in the universe when the phase transition completes. For this purpose, we examine when evolution of the scalar field becomes deterministic and estimate the power spectrum of quantum fluctuations. Finally, the result of numerical simulations on the spectrum of defects thus produced is presented and its analytic interpretation is given.

2.3 Evolution of the Scalar Fields

In this section, we trace the evolution of χ to discuss when its sign in each domain becomes fixed so that we may predict where topological defects will appear after completion of the phase transition. The symmetric state $\chi = 0$ becomes classically unstable when $\xi\mathcal{R}$ becomes smaller than λv^2. Evolution of the scalar field after this epoch can be divided to two stages. In the first stage, when its potential at the origin is still nearly flat, quantum fluctuations govern its evolution and its amplitude grows gradually. In the second stage typical amplitudes of χ become so large that its dynamics may be determined classically and its fate in each domain becomes predictable. We may regard the sign of χ as fixed in most domains at this epoch and follow its evolution classically thereafter.

In terms of the mean square value of a scalar field Φ with a constant mass M[82],

$$\langle\Phi^2(t)\rangle \cong \begin{cases} \dfrac{3H^4}{8\pi^2M^2}\left[1 - \exp\left(-\dfrac{2M^2t}{3H}\right)\right] , & \text{for } M^2 > 0 \ , \\ \dfrac{H^3}{4\pi^2}t \ , & \text{for } M^2 = 0 \ , \\ \dfrac{3H^4}{8\pi^2|M^2|}\left[\exp\left(\dfrac{2|M^2|t}{3H}\right) - 1\right] , & \text{for } M^2 < 0 \ , \end{cases} \tag{2.19}$$

it has been naively concluded in earlier literature[72] that the first stage lasts while $|M_\chi^2| \lesssim H^2$, where M_χ^2 is the mass squared at the origin in the equation (2.17), because the linear growth of the mean square field with time is characteristic of the era dominated by long-wave quantum fluctuations. However, this criterion is not valid in the present case in which M_χ^2 is time-dependent.

In order to find a more appropriate way to estimate when the evolution of χ becomes deterministic, let us focus on its long-wavelength part which is responsible for the symmetry breaking and satisfies the Langevin equation :

$$\frac{d\chi}{du} = -\frac{V'(\chi)}{3H^2(u)} + \frac{f(u)}{H(u)} , \tag{2.20}$$

under the assumption of slow rolling, which is justified if $|M_\chi^2| \ll 9H^2$[83]. We have used a new time variable $u \equiv \ln a(t) - \ln a(t_i)$ which is the e-folding number of cosmic expansion from t_i to t. The Hubble parameter squared is given by $H^2(u) = H^2(0) - \frac{2}{3}m^2 u \equiv H_i^2 - \frac{2}{3}m^2 u$. In the right-hand-side of the equation (2.20), the first term represents classical potential force, while the second term stands for random quantum noise with the correlation :

$$\langle f(u_1) f(u_2) \rangle \cong \frac{H^4(u_1)}{4\pi^2}\delta(u_1 - u_2) . \tag{2.21}$$

From the symmetry, the mean value of the field equals zero, *i.e.*, $\langle\chi\rangle = 0$. Hence χ represents the fluctuation of χ itself.

The most explicit treatment of the dynamical evolution of χ is to consider the time evolution of the probability density function of χ at t, $P(\chi, t)$, which satisfy the normalization condition :

$$\int_{-\infty}^{+\infty} P(\chi, t) d\chi = 1 . \tag{2.22}$$

The Fokker-Planck equation for $P(\chi, t)$ is derived using the stochastic inflation method[83, 84, 85] from the equation (2.20) such as

$$\frac{\partial}{\partial u}P(\chi, t) = \frac{\partial}{\partial \chi}\left(\frac{1}{3H^2(u)}\frac{\partial V}{\partial \chi}P(\chi, t)\right) + \hbar\frac{H^2(u)}{8\pi^2}\frac{\partial^2}{\partial \chi^2}P(\chi, t) , \tag{2.23}$$

where we write down $\hbar$ explicitly to point out a quantum effect term. We can say that the phase transition ends when $P(\chi, t)$ shows two peaks of χ distribution at the true vacuums. However, it is difficult to solve the equation (2.23), we instead deal the behavior of the mean square of χ defined by

$$\langle\chi^2(u)\rangle \equiv \int_{-\infty}^{+\infty} \chi^2 P(\chi, t) d\chi \tag{2.24}$$

since it is proper measure for the characteristic amplitude of χ. The above Langevin equation (2.20) yields the subsequent equation of motion for $\langle\chi^2(u)\rangle$:

$$\frac{d}{du}\langle\chi^2(u)\rangle \cong -\frac{2M_\chi^2}{3H^2(u)}\langle\chi^2(u)\rangle + \frac{H^2(u)}{4\pi^2} , \tag{2.25}$$

where the term proportional to $\langle\chi^4(u)\rangle$ has been neglected, which is shown to be a good approximation at the end of this section. Again the first term of the right-hand-side is a classical potential force and the second term represents quantum diffusion without which the equation (2.25) would be the same as the classical equation of motion for χ^2. Thus by comparing magnitudes of the two terms, one may conclude whether the evolution of χ is dominated by the potential force or fluctuations in typical domains.

The equation (2.25) may readily be solved :

$$\langle\chi^2(u)\rangle = \left[\langle\chi^2(0)\rangle + \frac{H_i^2}{4\pi^2}\int_0^u e^{8\xi u'}\left(1 - \frac{2m^2u'}{3H_i^2}\right)^{\frac{\lambda v^2}{m^2}+2\xi+1} du'\right] e^{-8\xi u}\left(1 - \frac{2m^2u}{3H_i^2}\right)^{-\frac{\lambda v^2}{m^2}+2\xi} . \tag{2.26}$$

If $2m^2u \ll 3H_i^2$ and $m^2 \ll \lambda v^2$,

$$\left(1 - \frac{2m^2u}{3H_i^2}\right)^{\frac{\lambda v^2}{m^2}+2\xi+1} \approx \exp\left(-\frac{2\lambda v^2}{3H_i^2}u\right) , \tag{2.27}$$

and (2.26) reads

$$\begin{aligned}\langle\chi^2(u)\rangle \;\approx\; & \langle\chi^2(0)\rangle \exp\left[-\frac{2(12\xi H_i^2 - \lambda v^2)}{3H_i^2}u\right] \\ & + \frac{1}{4\pi^2}\frac{3H_i^4}{2(12\xi H_i^2 - \lambda v^2)}\left\{1 - \exp\left[-\frac{2(12\xi H_i^2 - \lambda v^2)}{3H_i^2}u\right]\right\} .\end{aligned} \tag{2.28}$$

Since $12\xi H_i^2 - \lambda v^2$ is equal to the mass squared of χ, $M_\chi^2(u = 0)$, the above result is equivalent to that with a constant mass $M_\chi(u = 0)$ calculated by the one-loop field theoretic method in de Sitter spacetime (2.19). The equivalence between the stochastic inflation method and the field theoretic method has been discussed in[85]. With approximation (2.27), $\langle\chi^2(u)\rangle$ may increase or decrease depending on the sign of $12\xi H_i^2 - \lambda v^2$ or the choice of t_i.

We should hence consider higher-order terms in order to discuss transition to the second stage. Let us first consider the last exponent of the equation (2.26),

$$e^{-8\xi u}\left(1 - \frac{2m^2u}{3H_i^2}\right)^{-\frac{\lambda v^2}{m^2}+2\xi} \equiv G(u) . \tag{2.29}$$

We can expand $\ln G(u)$ as

$$\ln G(u) \;=\; -8\xi u + \frac{\lambda v^2 + 2\xi m^2}{m^2}\left[\frac{2m^2}{3H_i^2}u + \frac{1}{2}\left(\frac{2m^2}{3H_i^2}u\right)^2 + \frac{1}{3}\left(\frac{2m^2}{3H_i^2}u\right)^3 + ...\right]$$

$$= \frac{2(\lambda v^2 + 2\xi m^2 - 12\xi H_i^2)}{3H_i^2}u + \frac{2m^2(\lambda v^2 + 2\xi m^2)}{9H_i^4}u^2 + \frac{\lambda v^2 + 2\xi m^2}{3m^2}O\left(\left(\frac{2m^2}{3H_i^2}u\right)^3\right) . \quad (2.30)$$

The approximation (2.27) corresponds to adopting only the first term of (2.30). However, in the case where $M_\chi^2(u=0) = 12\xi H_i^2 - 2\xi m^2 - \lambda v^2$ is small, in which we are interested, the second term may dominate the first one and $G(u)$ grows. For simplicity, let us choose t_i so that $M_\chi^2 = 0$ or

$$H_i^2 = \frac{(\lambda v^2 + 2\xi m^2)}{12\xi} \quad (2.31)$$

at that time. Then for small u, $G(u)$ is given by

$$G(u) \cong \exp\left[\frac{32\xi^2 m^2}{\lambda v^2 + 2\xi m^2}u^2\right] . \quad (2.32)$$

Thus $G(u)$ starts to grow exponentially at $u \cong u_f$ with

$$u_f \equiv \sqrt{\frac{\lambda v^2}{32\xi^2 m^2}} = \sqrt{\frac{C}{32\xi^2}} , \qquad C \equiv \frac{\lambda v^2}{m^2} . \quad (2.33)$$

Similarly the integrand of (2.26), which is denoted $F(u')$, may be approximated as

$$\begin{aligned} \ln F(u') &= -\frac{2m^2(m^2 + 2\xi m^2 + \lambda v^2)}{9H_i^4}\left[u + \frac{3H_i^2(\lambda v^2 + m^2 + 2\xi m^2 - 12\xi H_i^2)}{2(m^2 + 2\xi m^2 + \lambda v^2)m^2}\right]^2 \\ &\quad + \frac{(\lambda v^2 + m^2 + 2\xi m^2 - 12\xi H_i^2)^2}{2(m^2 + 2\xi m^2 + \lambda v^2)m^2} - \frac{\lambda v^2 + m^2 + 2\xi m^2}{3m^2}O\left(\left(\frac{2m^2}{3H_i^2}u\right)^3\right) \\ &\cong -\frac{32\xi^2 m^2}{\lambda v^2}\left(u + \frac{1}{8\xi}\right)^2 + \frac{m^2}{2\lambda v^2} , \end{aligned} \quad (2.34)$$

where in the last expression we have used our assumption $\lambda v^2 \gg m^2$. Thus the integral yields

$$\int_0^u F(u')du' \approx \begin{cases} u & u \lesssim u_f , \\ u_f & u \gtrsim u_f . \end{cases} \quad (2.35)$$

The next task is to estimate $\langle\chi^2(0)\rangle$, which may depend on the initial state of the universe in general. One may expect, however, that the amplitude of $\langle\chi^2\rangle$ is $O((H/2\pi)^2)$ at the epoch when $M_\chi^2 = H^2$, independent of the initial condition, if the inflationary expansion lasts long enough by that time. We have numerically calculated $\langle\chi^2(0)\rangle$ using (2.26) starting with this condition for various values of $C = \lambda v^2/m^2$ ranging from 5 to 200 and $\xi = 3/16$. (The

reason why we adopted 3/16 for ξ is that it simplifies the calculations. The concrete formula will become evident in the next section.) As a result the inequality :

$$\langle\chi^2(0)\rangle \lesssim \frac{H_i^2}{4\pi^2}\sqrt{\frac{\lambda v^2}{m^2}} , \quad (2.36)$$

was always satisfied. Hence $\langle\chi^2(0)\rangle$ is unimportant in (2.26) for $u \gtrsim u_f$ and we may conclude

$$\langle\chi^2(u)\rangle \approx \frac{H_i^2}{4\pi^2}\sqrt{\frac{\lambda v^2}{32\xi^2 m^2}}\exp\left(\frac{32\xi^2 m^2}{\lambda v^2}u^2\right) . \quad (2.37)$$

Inserting this into the equation (2.25), we find that classical potential force begins to dominate quantum fluctuation at $u \approx u_f$.

The condition $u = u_f$ is realized at

$$t = t_i + \frac{3}{m}\left(\frac{C + 2\xi}{12\xi} - \sqrt{\frac{C}{12\xi} + \frac{1}{6} - \frac{1}{6\xi}\sqrt{\frac{C}{2}}}\right) \equiv t_f , \quad (2.38)$$

when the Hubble parameter,

$$H = m\sqrt{\frac{C}{12\xi} + \frac{1}{6} - \frac{1}{6\xi}\sqrt{\frac{C}{2}}} \equiv H_f , \quad (2.39)$$

is related with M_χ^2 as

$$\frac{H_f^2}{|M_\chi^2|} = \frac{1}{12\sqrt{2}\xi}\left(\sqrt{C} - \sqrt{2} + \frac{2}{\sqrt{C}}\xi\right) . \quad (2.40)$$

One can estimate the e-folding number of inflation after $t = t_f$ as

$$n_{fe} = \frac{3}{2m^2}\left(H_f^2 - \frac{m^2}{3}\right) = \frac{c}{8\xi} - \frac{1}{4} - \frac{1}{4\xi}\sqrt{\frac{c}{2}} . \quad (2.41)$$

In order that topological defects, which are thus produced, may leave observable traces, n_{fe} should be smaller than ≈ 60, otherwise they are inflated away from the present horizon. Hence this sets an upper bound on C. On the other hand, it should be at least larger than zero for the above arguments to be valid. Thus C should satisfy the following inequality for $\xi = 3/16$.

$$3 \lesssim C \lesssim 90 . \quad (2.42)$$

So far we have entirely neglected contribution of $\langle\chi^2(u)\rangle$ to M_χ^2 and the term proportional to $\langle\chi^4(u)\rangle = O(\langle\chi^2(u)\rangle^2)$ in (2.25). It is justified if

$$\lambda\langle\chi^2(u)\rangle \approx \frac{\lambda^2 v^2}{128\sqrt{2}\pi^2\xi^3}\sqrt{\frac{\lambda v^2}{m^2}} \lesssim m^2 , \quad (2.43)$$

which we may regard as a constraint on λ :

$$\lambda \lesssim 128\sqrt{2}\pi^2\xi^3 C^{-\frac{3}{2}} . \tag{2.44}$$

It is easy to satisfy the above inequality. Even if we take a rather large value of C, say $C = 90$, it only requires that $\lambda \lesssim 10^{-2}$ when $\xi = 3/16$.

2.4 Power Spectrum of Fluctuations

Here we deduce the formula for the spectrum of the mode function of χ at arbitrary time. Had there been no correlation beyond the Hubble horizon, we could have identified the correlation length of the phase transition with the Hubble length at the time when the phase transition finishes. However, the scalar field is correlated on various scales due to the inflationary expansion, which is characterized by the power spectrum $|\chi_k|^2$ of long-wave quantum fluctuations given in terms of mode function $\chi_k(t)$. Here we are going to calculate it.

The equation of motion for χ is

$$\begin{aligned} &\Box\chi + \frac{d}{d\chi}V[\chi] = 0 \\ \Longrightarrow\ &\left[\left(\frac{\partial}{\partial t}\right)^2 + 3H\frac{\partial}{\partial t} - \frac{\nabla^2}{a^2(t)}\right]\chi(\mathbf{x},t) + V'[\chi] = 0 . \end{aligned} \tag{2.45}$$

At first we decompose the operator χ as

$$\chi(\mathbf{x},t) = \int \frac{d^3k}{(2\pi)^3}[a_{\mathbf{k}}\chi_k(t)e^{i\mathbf{kx}} + a^+_{\mathbf{k}}\chi^*_k(t)e^{-i\mathbf{kx}}] , \tag{2.46}$$

where a_k and a^+_k are annihilation and creation operators, respectively. The mode function satisfies the following equation of motion :

$$\ddot{\chi}_k(t) + 3H\dot{\chi}_k(t) + \left(\frac{k}{a(t)}\right)^2\chi_k(t) + M^2_\chi\chi_k(t) = 0 . \tag{2.47}$$

Using a new variable $\tilde{\chi}_k \equiv a^{\frac{3}{2}}(t)\chi_k$ the above equation is rewritten as

$$\left[\frac{\partial^2}{\partial t^2} + \left(\frac{k}{a(t)}\right)^2 + M^2_\chi - \frac{3}{2}\dot{H} - \frac{9}{4}H^2\right]\tilde{\chi}_k = 0 . \tag{2.48}$$

In the inflationary stage, when the slow rolling condition $|\dot{H}| \ll H^2$ is applicable, we may regard the Hubble parameter to be constant over several expansion time scales during which

the physical wave number $k/a(t)$ decreases exponentially. Moreover since we are interested in the regime $|M^2_\chi| \lesssim H^2$ where quantum fluctuations are important, equation (2.48) can be approximately solved by the Hankel function of rank 3/2 and the positive frequency mode corresponding to that in the Minkowski vacuum for $k \gg Ha(t)$ reads

$$\tilde{\chi}_k(t) \cong \sqrt{\frac{\pi}{4H}}H^{(1)}_{\frac{3}{2}}\left(\frac{k}{Ha(t)}\right) , \tag{2.49}$$

where the mode function $\tilde{\chi}_k(t)$ is appropriately normalized according to

$$\tilde{\chi}_k(t)\dot{\tilde{\chi}}^*_k(t) - \tilde{\chi}^*_k(t)\dot{\tilde{\chi}}_k(t) = i . \tag{2.50}$$

While the above expression (2.49) is a good approximation, the comoving mode k can shift from short-wavelength regime to long-wavelength regime. In the latter phase, in which $(k/a(t))^2$ is negligible in (2.48), one may solve it by means of the WKB method[86] :

$$\tilde{\chi}_k(t) \cong A_k a^{\frac{3}{2}}(t_k)\left(\frac{S(t_k)}{S(t)}\right)^{\frac{1}{2}}\exp\left[\int^t_{t_k}S(t')dt'\right] + B_k a^{\frac{3}{2}}(t_k)\left(\frac{S(t_k)}{S(t)}\right)^{\frac{1}{2}}\exp\left[-\int^t_{t_k}S(t')dt'\right] , \tag{2.51}$$

where

$$S(t) \equiv \frac{3}{2}H\left(1 - \frac{4M^2_\chi}{9H^2} + \frac{2\dot{H}}{3H^2}\right)^{\frac{1}{2}} \cong \frac{3}{2}H . \tag{2.52}$$

The WKB approximation is valid provided $|\dot{S}| \ll S^2$. In the present model $S(t)$ is explicitly written as

$$S(t) = \frac{3}{2}H(t)\left(1 - \frac{16}{3}\xi + \frac{(8\xi-2)m^2 + 4\lambda v^2}{9H^2(t)}\right)^{\frac{1}{2}} . \tag{2.53}$$

In the case $\xi = 3/16 = 0.1875$, which is slightly larger than the conformally coupled case $\xi = 1/6 = 0.166...$, $S(t)$ is time-independent :

$$S = \sqrt{\lambda v^2 - \frac{3}{8}m^2} . \tag{2.54}$$

We will mainly study this case in the following for simplicity and this is why we have taken $\xi = 3/16$ in the previous section.

The coefficients A_k and B_k may be determined by the initial condition at $t = t_k$ and the normalization condition. One may determine the coefficient of the leading term A_k with the help of (2.49), which is explicitly written as

$$\begin{aligned} \tilde{\chi}_k(t) &\cong -i\left(\sqrt{\frac{H^2}{2k^3}}a^{\frac{3}{2}}(t) - \frac{i}{\sqrt{2k}}a^{\frac{1}{2}}(t)\right)e^{-i\frac{k}{Ha(t)}} \\ &\approx -i\sqrt{\frac{H^2}{2k^3}}a^{\frac{3}{2}}(t) , \end{aligned} \tag{2.55}$$

where the last expression is the approximate solution for the case the physical wavelength of the k-mode is larger than the horizon scale ($k \lesssim aH$). With the approximation $S(t) \cong \frac{3}{2}H(t)$, the equation (2.51) reads

$$\tilde{\chi}_k(t) \cong A_k a^{\frac{3}{2}}(t_k) \exp\left[\frac{3}{2}H(t-t_k)\right] \cong A_k a^{\frac{3}{2}}(t) \ . \tag{2.56}$$

Thus from (2.55) and (2.56) we can determine A_k as

$$A_k = \sqrt{\frac{H^2(t_k)}{2k^3}} \ , \tag{2.57}$$

where the unimportant phase factor has been omitted. Thus the mode function in the long-wavelength regime is given as

$$\chi_k(t) \cong \sqrt{\frac{H^2(t_k)}{2k^3}} \left(\frac{S(t_k)}{S(t)}\right)^{\frac{1}{2}} \left(\frac{a(t_k)}{a(t)}\right)^{\frac{3}{2}} \exp\left[\int_{t_k}^{t} S(t')dt'\right] \ . \tag{2.58}$$

One may get this result independently of the choice of the connecting time t_k as far as both (2.49) and (2.51) are reasonable approximations at $t = t_k$. Hereafter we take t_k to be the epoch the k-mode leaves the de Sitter horizon, that is,

$$k = H(t_k)a(t_k) \equiv H_k a_k \ . \tag{2.59}$$

Depending on the value of ξ, the equation (2.58) reads

$\circ\ \xi = \frac{3}{16}$

$$\chi_k(t) = \exp\left[-\frac{9}{4m^2}\left(H_k^2 - H^2\right) + \frac{9}{2m^2}\sqrt{\beta}\,(H_k - H)\right]\frac{H_k}{\sqrt{2k^3}} \ , \tag{2.60}$$

$\circ\ \xi < \frac{3}{16}$

$$\begin{aligned}\chi_k(t) \ &= \ \exp\left[-\frac{9}{4m^2}\left(H_k^2 - H^2\right) - \frac{9\sqrt{\alpha}}{4m^2}\left(H\sqrt{H^2+\beta\alpha} - H_k\sqrt{H_k^2+\frac{\beta}{\alpha}}\right)\right] \\ &\times \left(\frac{\alpha H_k^2+\beta}{\alpha H^2+\beta}\right)^{\frac{1}{4}} \left(\frac{H+\sqrt{H^2+\frac{\beta}{\alpha}}}{H_k+\sqrt{H_k^2+\frac{\beta}{\alpha}}}\right)^{-\frac{9\beta}{4\sqrt{\alpha}m^2}} \frac{H_k}{\sqrt{2k^3}} \ ,\end{aligned} \tag{2.61}$$

$\circ\ \xi > \frac{3}{16}$

$$\chi_k(t) = \exp\left[-\frac{9}{4m^2}\left(H_k^2 - H^2\right)\right]\left(\frac{\beta - |\alpha|H_k^2}{\beta - |\alpha|H^2}\right)^{\frac{1}{4}} \frac{H_k}{\sqrt{2k^3}} \times \tag{2.62}$$

$$\exp\left[-\frac{9\sqrt{|\alpha|}}{4m^2}\left(H\sqrt{\frac{\beta}{|\alpha|}-H^2} + \frac{\beta}{|\alpha|}\sin^{-1}\frac{H}{\sqrt{\beta/|\alpha|}} - H_k\sqrt{\frac{\beta}{|\alpha|}-H_k^2} - \frac{\beta}{|\alpha|}\sin^{-1}\frac{H_k}{\sqrt{\beta/|\alpha|}}\right)\right] \ ,$$

where $H = H(t)$ and the parameters are defined as

$$\alpha = 1 - \frac{16}{3}\xi \ , \quad \frac{\beta}{m^2} = \frac{4}{9}C - \frac{2}{9}(1-4\xi) \ . \tag{2.63}$$

For the case $\xi = 3/16$, the mode function begins growing at

$$H(t) = \frac{2}{3}\sqrt{\lambda v^2 - \frac{m^2}{8}} \equiv H_c \tag{2.64}$$

at which epoch $M_\chi^2 = -\frac{m^2}{2}$. Because of the gradual decrease of the Hubble parameter, it is slightly after $\chi = 0$ becomes unstable that χ_k starts to grow.

The amplitude of (2.60) in the case $\xi = 3/16$ and $C = 5$ is shown in Figure 2.1, which depicts relative amplitude to that of a massless minimally-coupled scalar field in the exact de Sitter spacetime given by $(H_f^2/2k^3)^{\frac{1}{2}}$.

2.5 Distribution of the Topological Defects

2.5.1 Numerical Simulations

Having estimated when evolution of χ becomes dominated by the potential force in the section 2.3 and calculated the power spectrum of its fluctuations at an arbitrary time in the section 2.4, we are now in a position to apply them to find the spectrum of topological defects produced. Following our two step approximation described in the section 2.3, this is accomplished by calculating spatial distribution of the scalar field at $t = t_f$. Thanks to the properties of the vacuum state realized as a result of inflationary expansion, $\chi(\mathbf{x}, t_f)$ is classically given by summing up its Fourier modes as

$$\chi(\mathbf{x}, t_f) = \sum_{\mathbf{k}} \delta\chi_{\mathbf{k}}(\mathbf{x}, t_f) + \text{C.C.} \ ; \delta\chi_{\mathbf{k}}(\mathbf{x}, t_f) = |\delta\chi_k(t_f)|e^{i\mathbf{k}\mathbf{x}+i\varphi_{\mathbf{k}}} \ , \tag{2.65}$$

where $|\delta\chi_{\mathbf{k}}(t_f)|$ is a random value which has a Gaussian distribution with dispersion $|\chi_k(t_f)|^2$ and $\varphi_{\mathbf{k}}$ is a random phase-factor.

If we find the sign of χ positive (negative) at a certain point at $t = t_f$, it will fall down to the minimum of $\chi = +v$ $(-v)$ as the phase transition proceeds, since its dynamics has been deterministic by this time in typical domains. Thus we may consider that domain walls are produced between two regions with opposite signs of χ at this time.

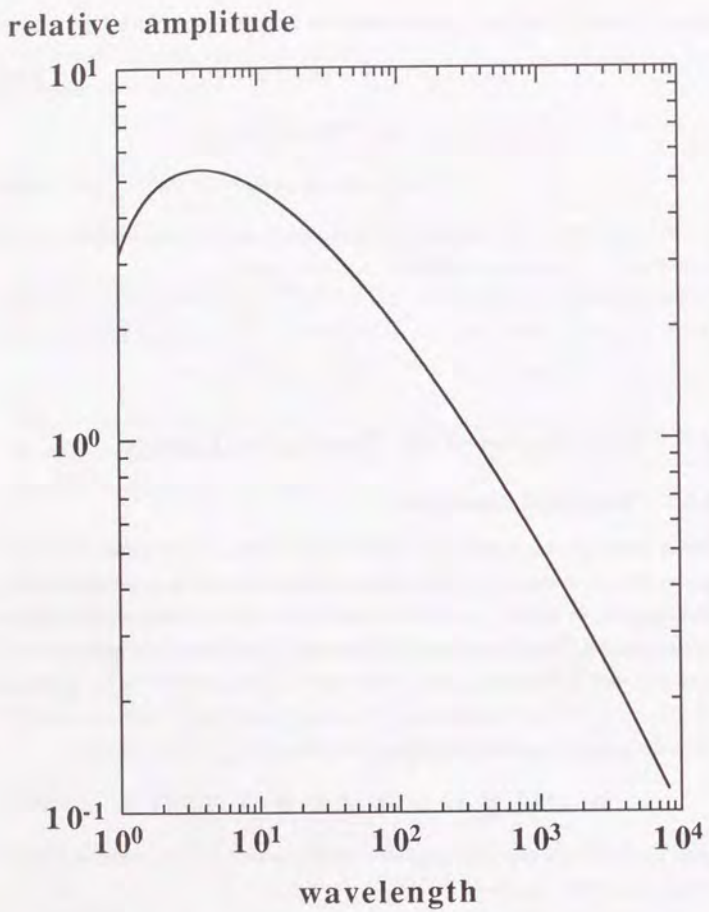

Figure 2.1: Magnitude of the mode function $|\chi_k(t_f)|$ for $\xi = \frac{3}{16}$ and $C = 5$ as expressed in the equation (2.60). Plotted values are relative amplitude to $(H_f^2/2k^3)^{\frac{1}{2}}$. Abscissa corresponds to the wavelength $2\pi a(t_f)/k$ in unit of H_f^{-1}.

We have first done three-dimensional simulations as illustrated in Figure 2.2, in which we have calculated the value of $\chi(\mathbf{x}, t_f)$ through the equation (2.65) at each point of 32^3 lattices using the power spectrum of χ_k with $\xi = 3/16$ and $C = 5$. We adopted the fast Fourier-transform(FFT) method to speed up the calculation[87] and summed up 32^3 modes of $\delta\chi_{\mathbf{k}}$ with k ranging from $2\pi H_f/32$ to $2\pi H_f$, where H_f^{-1} is the separation of neighboring lattice-points taken to be the Hubble length at $t = t_f$. In the figure marked points will fall in the plus minimum or $\chi = v$ and unmarked points in the minus minimum after the phase transition so that domain walls will be present between them. As is seen there, there are structures on various scales. This is in contrast to Figure 2.3, in which the sign of χ has been randomly assigned to each lattice-point corresponding to the case of a thermal phase transition with the correlation length H_f^{-1}.

In both cases, however, simulation boxes are dominated by walls with infinitely large surface area. This is simply because both states of $\chi = \pm v$ are realized with equal probability and hence it is unlikely that walls are so distributed that islands of plus minimum exist in the sea of minus minimum or vice versa. Thus it is not appropriate to examine the area-distribution of walls in order to discuss the character of phase transitions.

Hence we instead focus on distribution of separation of each wall. For this purpose we do not have to calculate the value of the equation (2.65) at all points in three dimensional space. But all we should find is its value along a line, which enables us to employ a much larger simulation box. In fact we have used a box with $(2^{13})^3$ lattice points and examined the distribution of domains along a line with 2^{13} points. We have done simulations for the following two cases :

- A. Power spectrum is given by the equation (2.60) with $\xi = 3/16$ and $C = 5$.
- B. A scale-invariant power spectrum,

$$|\chi_k|^2 = \frac{H_f^2}{2k^3} ,$$

is assigned corresponding to the case with a massless scalar field in de Sitter spacetime.

In both cases we have summed $2^{13} \times 100 = 819200$ independent mode functions in the equation (2.65) with k ranging from $2\pi H_f/2^{13}$ to $2\pi H_f$. Simulations have also been done in the case a box with $(2^{12})^3$ points. As a result no artificial boundary effect was observed.

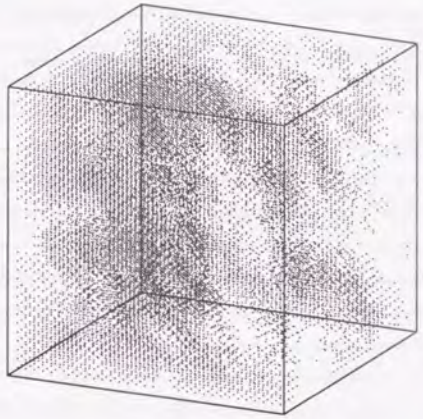

Figure 2.2: Distribution of domains in plus vacuum. Marked points depict regions with $\chi = +v$. Values of the field are determined by giving correlations specified by the spectrum in the equation (2.60). The box size is 32^3 and lattice separation is equal to H_f^{-1}.

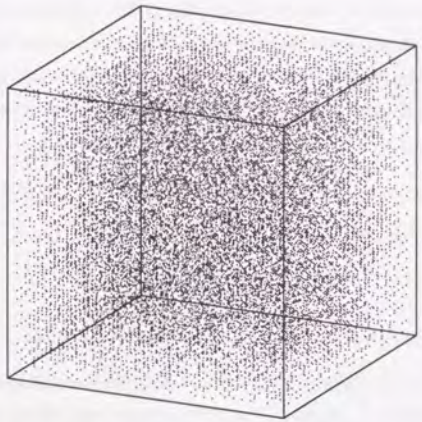

Figure 2.3: Same as Figure 2.2 but the sign of χ at each point is given randomly.

In addition simulations in which the upper bound of k is taken to be πH_f have been carried out and no effect of small-scale cutoff emerged. For comparison we have also studied the case :

- C. Sign of χ is assigned at random at each point.

We have done simulations for 500 times for each case and their results are depicted in Figure 2.4. We can obtain various consequences from the graph. As is seen there domain-size distribution in phase transition during the inflation (A and B) is again very different from that in thermal phase transition (C). In the latter case we can fit the distribution with an exponential function :

$$n(s,t_f)ds \;\propto\; \exp(-0.67s)ds \;, \tag{2.66}$$

where $n(s,t_f)$ is the number density of domains with separation $s \sim s+ds$. This is simply because the number of domains with size sH_f^{-1} is proportional to the probability of having the same sign of χ for s times in succession :

$$n(s,t_f)ds \;\propto\; \left(\frac{1}{2}\right)^s ds \;\propto\; \exp(-\ln 2 \cdot s)ds \;\propto\; \exp(-0.69s)ds \;.$$

Thus our numerical simulation agrees with the analytic estimate.

On the other hand, in the case B we may fit the distribution with a power-law :

$$n(s,t_f)ds \;\propto\; s^{-p}ds \;, \qquad \text{with} \;\; p = 3.0 \;. \tag{2.67}$$

We can extend the above one-dimensional result into three dimension as follows. First let us define the effective correlation volume of a domain between two walls with separation s by $V \equiv s^3$. Then, since the probability to find a structure with this correlation volume by our simulation is proportional to its effective surface area or s^2, number density of domains with correlation volume V, $n(V,t_f)$, is related to $n(s,t_f)$ by

$$n(s,t_f)ds \;\propto\; n(V,t_f)s^2ds \propto n(V,t_f)dV \propto V^{-5/3}dV \;. \tag{2.68}$$

Thus the surface area density of walls, $\sigma(V,t_f)$, is given by

$$\sigma(V,t_f)dV \;\propto\; n(V,t_f)V^{2/3}dV \;\propto\; V^{-1}dV \;. \tag{2.69}$$

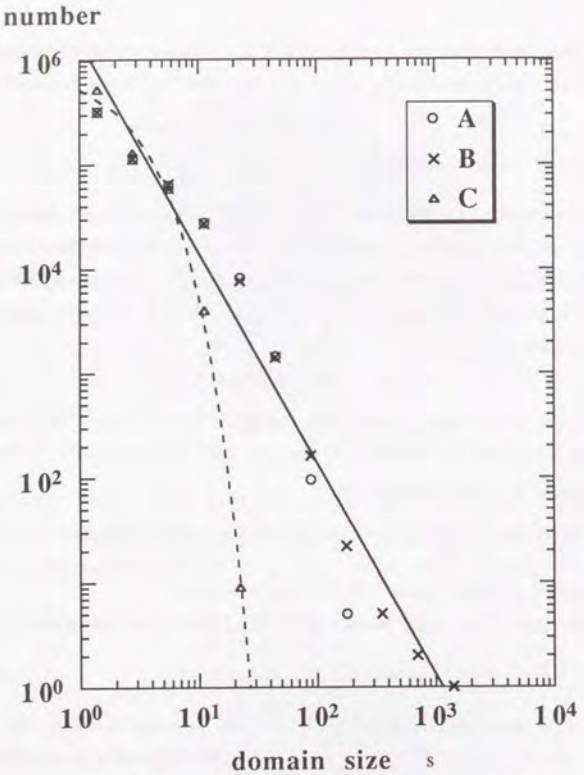

Figure 2.4: Distribution of the separation of domain walls. This figure shows the sum of 500 times simulations of the length 2^{13}. Plotted values are integrated one in each logarithmic interval.

A(○): $\chi(\mathbf{x}, t_f)$ is calculated using the power spectrum given by the equation (2.60).

B(×): $\chi(\mathbf{x}, t_f)$ is calculated using the scale-invariant power spectrum. Solid line is the power-law fitting whose power index becomes -2.0 due to integration by s.

C(△): The sign of $\chi(\mathbf{x}, t_f)$ is assigned randomly with equal probability corresponding to the thermal phase transition with correlation length H_f^{-1}. The plot fits an exponential function depicted by the dashed line.

Therefore in the case that a scale-invariant fluctuation is assigned, we find that the energy spectrum of the resultant topological defects is also scale-invariant. Analytic arguments to derive this distribution will be given in the next subsection.

Finally the open circles A in Figure 2.4, for which the more realistic spectrum has been assigned, shows almost the same profile as the crosses B for $s \lesssim 80$ but larger domains are suppressed because amplitudes of fluctuations with larger wavelength are smaller. From Figures 2.1 and 2.4 we may conclude the fluctuation mode with $\sqrt{k^3|\chi_k(t_f)|^2}$ smaller than $\sim 10\%$ of its maximum is unimportant and the spectrum of topological defects on such a large scale should approach that predicted by white-noise fluctuations.

2.5.2 Analytical Interpretaion

Here let us consider how the above scale-invariant feature of topological defects is explained analytically. To make the following discussion simple and clear let us focus on a patch of space which was homogeneous with $\chi = 0$ at $t = 0$. Let us further assume that the space may be divided into many domains of horizon volume H^{-3} with different values of χ at each time. Then the probability distribution function of χ is given by

$$P[\chi(\mathbf{x}, t) = \chi] = \frac{1}{\sqrt{2\pi G(0,t)}} \exp\left[-\frac{\chi^2}{2G(0,t)}\right]; \qquad G(0,t) = \langle \chi^2(\mathbf{x}, t)\rangle = \frac{H^2}{4\pi^2} Ht \ . \quad (2.70)$$

Furthermore joint probability distribution reads

$$P[\chi(\mathbf{x}_i, t) = \chi_i; \chi(\mathbf{x}_j, t) = \chi_j] = \frac{1}{2\pi G(0,t)\sqrt{1-\rho^2(r,t)}} \exp\left\{-\frac{\chi_i^2 + \chi_j^2 - 2\rho(r,t)\chi_i\chi_j}{2G(0,t)[1-\rho^2(r,t)]}\right\} , \quad (2.71)$$

where $\rho(r,t) \equiv G(r,t)/G(0,t) = \langle \chi(\mathbf{x}_i, t)\chi(\mathbf{x}_j, t)\rangle / G(0,t)$ with $|\mathbf{x}_i - \mathbf{x}_j| = r$. The condition for existence of a wall at a certain point is that χ changes its sign there, whose probability, $F(t)$, is given by

$$\begin{aligned} F(t) &\equiv \int_{-\infty}^{0} d\chi_i \int_0^{+\infty} d\chi_j 2P[\chi(\mathbf{x}_i, t) = \chi_i; \chi(\mathbf{x}_j, t) = \chi_j]; \qquad |\mathbf{x}_i - \mathbf{x}_j| = H^{-1}, \\ &= \frac{1}{\pi} \arccos\left[\frac{G(H^{-1}, t)}{G(0,t)}\right] \cong \frac{1}{\pi} \arccos\left(1 - \frac{1}{Ht}\right) \cong \frac{1}{\pi}\sqrt{\frac{2}{Ht}} , \end{aligned} \quad (2.72)$$

where the last approximation is justified if $Ht \gg 1$. Thus $F(t)$ depends on t only weakly even though the background space is expanding exponentially.

Thanks to the assumption of homogeneity at $t = 0$, the largest possible wall at time t has a physical size of $V = H^{-3}e^{3Ht}$, so that $F(t)$ is related with $\sigma(V,t)$ as

$$F(t) \approx H^{-1} \int_{H^{-3}}^{H^{-3}e^{3Ht}} \sigma(V,t) dV \ , \tag{2.73}$$

where the $t-$dependence of $\sigma(V,t)$ reflects the fact that quantum fluctuations are generated continuously to produce and destroy topological defects successively in the course of cosmic expansion. Since this is a rather stationary process without any exponential instability, $\sigma(V,t)$ should not depend on t exponentially just as $F(t)$ does not. Furthermore the fact that our numerical results were insensitive to the upper bound of k implies that $F(t)$ should not strongly depend on the lower bound of the integral in (2.73). Thus we expect from (2.73) that $\sigma(V,t)$ should be proportional to V^{-1} to eliminate the exponential dependence on t of the upper bound of the integral and to avoid strong dependence on the lower bound. In this way we conclude that distribution of walls is scale-invariant and given by

$$\sigma(V,t)dV \approx \frac{H}{(Ht)^{\frac{3}{2}}} \frac{dV}{V} \ , \tag{2.74}$$

for $Ht \gg 1$.

2.6 Discussion

We have studied generic features of a second-order phase transition during the inflation which is a more natural and attractive scenario to produce topological defects at GUT scale than the Kibble mechanism. We have considered a specific model in which χ is coupled with spacetime curvature $\mathcal{R}$ and a phase transition occurs due to gradual decrease of the Hubble parameter. In this model we have clarified the nature of long-wavelength quantum fluctuations by explicitly calculating the power spectrum and $\langle \chi^2 \rangle$.

In terms of the latter quantity we determined when the classical potential force surpasses quantum fluctuations in typical domains and investigated the distribution of the field at that epoch through numerical calculations, by which we examined distribution of topological defects.

As a result we have found that they have an almost scale-invariant distribution with small- and large-scale cutoffs. The former is naturally given by the comoving scale corresponding to the Hubble radius at the epoch time evolution of χ becomes dominated by the

classical potential force, while our simulations have shown that the latter corresponds to the scale on which the amplitude $\sqrt{k^3|\chi_k(t_f)|^2}$ of fluctuations becomes smaller than $\sim 10\%$ of its maximum value as is seen in Figures 2.1 and 2.4. On the larger scale the fluctuation amplitude becomes so small that the distribution should approach white-noise spectrum.

Note that though Hodges and Primack[80] reported similar results, *i.e.*, scale-invariant distribution of topological defects produced during the inflation, their treatment is not adequate in two aspects. First they have assumed that topological defects with a certain comoving scale are produced only when that scale leaves the Hubble radius during the inflation. Contrary to their approximation, however, significant amount of defects could be produced and destroyed on various scales continuously through successive generation of fluctuations as discussed in the section 2.5. Second they have not given cutoffs of the distribution explicitly. As is seen above we have significantly improved these points through our analyses.

Finally we stress that our basic results are also applicable to other topological defects such as strings or textures in which we are more interested[80]. For example, strings are loci on which both real and imaginary parts of string-forming complex scalar field changes sign. Hence if the self-coupling λ of the field is small enough we can identify strings with intersections of two different kinds of independent "domain walls." Thus with the same reasoning as the subsection 2.5.2 they also have a scale-invariant distribution with cutoffs. Furthermore, since the model parameters must satisfy

$$\frac{\lambda v^2}{m^2} \lesssim 90 \tag{2.75}$$

in order that strings thus produced are not diluted too much by subsequent inflation, we have

$$\lambda \lesssim 10^{-4} \left(\frac{v}{10^{16}\mathrm{GeV}} \right)^{-2} \left(\frac{m}{10^{13}\mathrm{GeV}} \right)^{2} \ , \tag{2.76}$$

so that the condition of λ being small is automatically satisfied for cosmologically important strings.

Chapter 3

Wall-String Systems

The dynamical evolution of a wall-string system is investigated in this chapter. Walls intersect each other and collapse approximately at the speed of the light velocity. Such moving walls attract matter as positive gravitational sources in contrast to static walls. They annihilate with few oscillation so that the lost energy radiates as a scalar mode. Thus although the decays are non-spherical, the production of gravitational waves is expected to be rare. As for the $N = 1$ axion domain wall model, walls prove to be harmless in the standard cosmology since they do not dominate the universe.

3.1 The Axion Model

The axion is a pseudo-Nambu-Goldstone boson that is postulated in order to solve the CP invariance problem in the strong interaction[46, 88]. The strong CP problem[89] is a theoretical problem, which arises from the fact that there are degenerate multiple vacuums in the quantum chromodynamics(QCD). On account of this non-perturbative effect, a parameter representing the CP-violation enters the theory. The experimental constraint by an electric dipole moment for the neutron suggests that this parameter must be an extremely small number or zero. The most natural and popular solution to this problem is the Peccei-Quinn mechanism in which the Lagrangian is invariant under a global unitary transformation of degree one. This symmetry is called the Peccei-Quinn symmetry and we express it as $U(1)_{PQ}$. The $U(1)_{PQ}$ symmetry breaks spontaneously at the energy scale, f_a. The associated Nambu-Goldstone boson is the axion. Actually the axion gets its mass, m_a,

at the QCD scale from the instanton effect. The value of m_a is related to f_a as

$$m_a \simeq 0.62\text{eV}\left(\frac{10^7\text{GeV}}{f_a/N}\right) , \tag{3.1}$$

where an integer N is the color anomaly of the $U(1)_{PQ}$ symmetry.

The axion of arbitrary value of f_a can similarly resolve the strong CP problem. The amplitude of f_a must be determined by experiments although part of them depends on how the axion interacts with ordinary matter. The main constraints are from high energy accelerators, from astrophysical observations, especially the cooling effect of the axion emission on stellar evolution like red giants or supernovae explosion, and from the cosmological limit, not to dominate the energy density of the universe by axions from the thermal or non-thermal production including string decay. Hence the value of the axion mass, m_a, is strictly limited to a narrow window[2] :

$$10^{-6}\text{ eV} \lesssim m_a \lesssim 10^{-3}\text{ eV} . \tag{3.2}$$

Particularly the lower limit is acquired from the constraint that the axions should not make the value of Ω_0 much greater than one. Thus if the axion mass takes the critical value, the universe can be flat. The axion is one of the most realistic candidates of the cold dark matter[90].

In addition to the role as a possible non-luminous matter, domain walls are produced in the axion model. Since the essence of the axion model is the additional global symmetry which breaks spontaneously, it will produce topological defects. They are complex defects in the sense that walls are bounded by strings. Two transitions of different energy scales are involved in the model. First, the $U(1)_{PQ}$ symmetry is broken to a circular vacuum and global strings are produced. Then through the second phase transition at QCD energy scale, the previous circular vacuum gains discrete N potential minima. Thus the strings come to be surrounded by N walls that spring out from each string. Besides the axion model may produce non-Gaussian fluctuations by global strings and domain walls[91] or the inflaton coupled to the axion field[92]. Thus the cosmological importance of the axion is profound.

For the axion model to work successfully, generated domain walls should vanish not to dominate the universe with their energy[93]. It is believed that in the cases of $N > 1$ the network of walls survives too long so that the model does not work, although the $N = 1$

walls rapidly disappear, which means the postulation of axions does not conflict with the cosmological observations. Ryden et al. obtained such results by counting the wall area evolution using the numerical data but they adopted a modified equation[94]. Moreover, in contrast to their simulation in which the box contains a great amount of walls, we have investigated the dynamics of an individual string-wall system by considering the detailed procedure of wall collapses[95] in section 3.3.

3.2 Model Lagrangian and Numerical Method

In the present chapter, we concentrate on walls bounded by strings motivated by the axion model. These hybrid topological defects are examined from two viewpoints for cosmological walls. One is concerning the property which makes the standard cosmology fail. We will try to justify the hypothesis that the $N = 1$ walls should be erased harmlessly. The other is about the advantage of walls which contributes the cosmological structure formation. It is checked how walls can give initial fluctuations for the matter accretion. With the purpose of clarifying above properties the fate of collapsing walls is simulated numerically.

We employ a complex scalar field of a single component that obeys a following Lagrangian with a U(1) breaking term :

$$\mathcal{L} = \frac{1}{2}|\partial_\mu \chi|^2 - V_s(\chi) - V_w(\chi)\ ,\quad V_s(\chi) = \frac{\lambda}{4}(|\chi|^2 - v^2)^2\ ,\quad V_w(\chi) = V_a(1 - \cos\theta_a)\ , \tag{3.3}$$

where θ_a signifies the phase of χ. The first term of the potential, V_s, gives rise to strings and domain walls ($N = 1$) at $\theta_a = \pi$ are originated from the second term, V_w. The line energy density of strings, μ, and the core radius of them, δ_s, are

$$\mu \sim v^2\ ,\quad \delta_s \sim 2(\lambda v^2)^{-1/2}\ , \tag{3.4}$$

respectively. The surface energy density of walls, σ, and the thickness scale of them, δ_w, are

$$\sigma \sim v\sqrt{V_a}\ ,\quad \delta_w \sim \frac{v}{\sqrt{V_a}}\ . \tag{3.5}$$

We have formulated these quantities already in the section 1.3.

In the case of the $N = 1$ axion model, v and V_a are related to the Peccei-Quinn symmetry breaking scale and the axion mass as

$$v = f_a\ ,\quad V_a = f_a^2 m_a^2\ . \tag{3.6}$$

Hence the wall thickness is the axion mass scale $\delta_w \sim m_a^{-1}$ and the surface energy density of the wall is in proportion to f_a.

After the first phase transition, the amplitude of the field should be the vacuum expectation value, v, in the region where no string exists. We can derive the exact static solution for an infinite plane wall when $|\chi| = v$ is satisfied. In the case that the wall spreads on the $yz-$plane, the equation for θ_a is written as

$$\frac{d^2}{dx^2}\theta_a - \frac{V_a}{v^2}\sin\theta_a = 0\ , \tag{3.7}$$

whose non-trivial solution is expressed as

$$\theta_a(x) = \pi + 2\sin^{-1}\left(\tanh\frac{x}{v/\sqrt{V_a}}\right)\ . \tag{3.8}$$

Such a configuration is used as an initial distribution of χ in numerical simulations performed in the section 3.3.

To follow the time evolution of walls numerically, we have to solve the field evolution under a certain spacetime. As the most simple hypothesis, we assume that the background is a flat Robertson-Walker universe. Then the field equation is written as

$$\frac{\partial^2\chi}{\partial\tau^2} + \frac{2}{a}\frac{da}{d\tau}\frac{\partial\chi}{\partial\tau} - \nabla^2\chi = -a^2\frac{\partial V}{\partial\chi}\ . \tag{3.9}$$

When we pay attention to a single string-wall system well inside the cosmological horizon, the effect of the cosmic expansion can be neglected. Thus we can make use of the Minkowski metric. Then the evolution equation is approximated as

$$\frac{\partial^2\chi}{\partial t^2} - \nabla^2\chi = -\frac{\partial V}{\partial\chi}\ . \tag{3.10}$$

In numerically solving processes, the calculations are interrupted by the factor, a^2, on the right-hand-side term of the equation (3.9). The physical meaning of this breakdown is that the resolution becomes lower with the increase of the expansion factor, a, since the lattice separation of the simulation box is constant in comoving size although the wall width is constant in physical length. To escape from this restriction, Ryden et al.[94] dropped the a^2 factor and replaced the coefficient, 2, in the second term of the left-hand-side in the equation (3.9) with 3. We are confident that this modification should alter the dynamics of walls fatally so we have used two equations (3.9) and (3.10) without any reformation.

Numerical simulations have been performed in two-dimensional and three-dimensional boxes. In both cases, the equation has been solved by a staggered leapfrog algorithm in a second-order accuracy[87]. Detailed formulas for solving these equations are the same as those in the case of global textures introduced in the next chapter. The parameters are set such that $\delta_s \sim 2$ meshes and $\delta_w \sim 10$ meshes. As a result, the ratio of the string vacuum energy to the wall vacuum energy, $\lambda v^4/V_s$, becomes ~ 100. This value should be large enough since we have found that the wall dynamics has not been affected even when μ was multiplied by ten. This is because there is extremely small region where the field stays in the false vacuum of V_s.

We have executed the computations under the periodic boundary in the section 3.4 and the free boundary, in which the gradient of the field is fixed, in the section 3.3. Other boundary conditions do not modify our conclusions since the box size is so large that the influence of the boundaries cannot reach where defects interact. When the cosmic expansion is taken into account, the scale-factor grows as $a \propto \tau$ like the law in the radiation dominated stage or $a \propto \tau^2$ like that in the matter dominated stage.

Since we have followed the evolution of the field itself, the viewpoint that walls are rigid thickless sheet is not necessary. We can follow the motion of walls using the distribution of the potential energy of domain walls, V_w, in the simulation box. The subsequent section treats walls of finite thickness and its behavior when walls collapse and disappear is examined in detail.

3.3 Dynamics of the Walls

3.3.1 Intersection of the Walls

In this section, we consider the interaction between two walls. First we can ignore the cosmic expansion and the equation (3.10) is adopted since defects fairly inside the horizon are considered. The initial condition is set so that one wall and one string-wall exist in the simulation box. Here "one wall" means the wall that has no end in the simulation box. And "one string-wall" means the wall that has only one end in the simulation box. They are arranged such that the edge of the string-wall faces one side of another wall. The distance

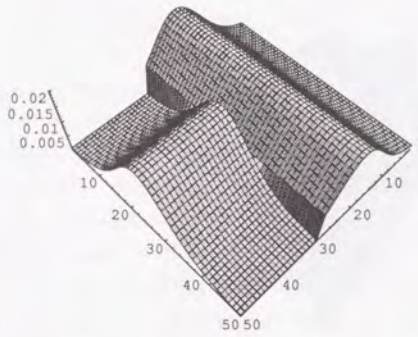

Figure 3.1: Two-dimensional distribution of the potential energy, V_w, in 50×50 $xy-$slice of a 100^2 simulation is shown. This is the initial configuration for the crash of a wall and a string-wall. The vertical axis is normalized as $V_s = 0.01$.

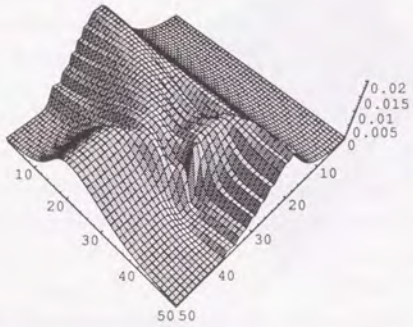

Figure 3.2: The value of V_w when the time, $t = 10\Delta/c$, has passed from the initial configuration is depicted.

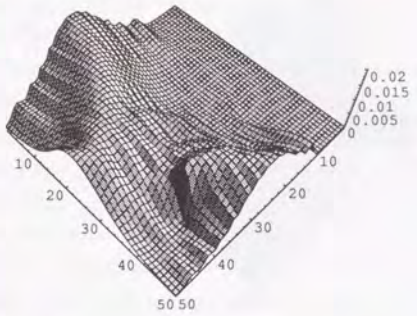

Figure 3.3: The value of V_w when the time, $t = 20\Delta/c$, has passed from the initial configuration is depicted.

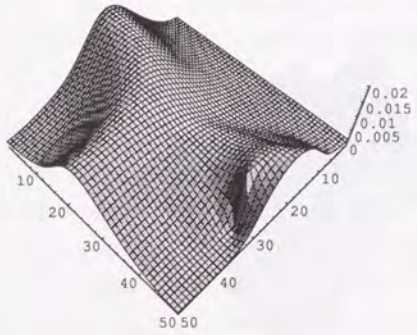

Figure 3.4: Spatial distribution of V_w when the scale-factor grows thirty times as much as the initial one is drawn. The calculation begins from the same configuration as the non-expanding case.

between them is 10 meshes. The translational symmetry in the $z-$direction is imposed on the configuration in the 100^2 box. For the spatial distribution of the phase of χ, θ_a, on both sides of each wall, we substitute a solution for an infinite planar wall under the approximation $|\chi| = v$ on the $yz-$plane in the equation (3.8). The initial distribution of V_w at the $(x, y)-$slice is shown in Figure 3.1. This figure picks up the 50×50 meshes in the central principal part. The initial configuration of χ does not satisfy the static equation for the field at the border where two walls meet since we deal with the drastic encounter of sub-horizon scale walls which have no causal contact each other in advance. In such cases, they should move drastically. Thus walls in simulations have an initial relative velocity whose magnitude is equal to the light velocity, c. Figure 3.2 shows the same quantity at the same slice as Figure 3.1 after the period of $10\Delta x/c$, where Δx represents the lattice separation. In this figure, the wall is cut by the string-wall and a kind of intercommutation of the walls is proceeding in the similar way as strings. The intercommutation of strings is calculated numerically both in a global string[96] and in a local one[97]. When $t = 20\Delta x/c$, the reconnection of walls makes further progress, which we can see in Figure 3.3. The speed of wall motion is estimated from the displacement of the string false vacuum to be about $0.5c$.

We have also checked how the behavior of the walls is altered when the cosmological expansion is included using the equation (3.9). The initial horizon equals to the grid length so that extreme super-horizon walls are assigned. It corresponds to the phase transition after or during the inflation in which the correlations of much larger scales than the Hubble length exist due to the exponential expansion of the universe which we have described in the chapter 2. The value of V_w after the scale-factor grows 30 times as large as the initial one is shown in Figure 3.4. The calculation in the radiation dominant era starts from the same initial setup as the non-expanding one. Since noisy modes are damped by the cosmic expansion, the intercommutation process can be seen more distinctly than Figure 3.3. However, the configuration of χ is practically unchanged from the onset of the simulation and the collapse of walls is still on the way at this time. The walls move at almost the speed of light but the introduction of the expansion decelerates the disintegration process. it takes a few decades of expansion times for the process to be accomplished. We have confirmed that more rapid expansion in the matter era decelerates such procedure more considerably.

3.3.2 Collapse of the Walls

After repeated intercommutations, walls are divided to multiple small pieces. To examine the fate of such a wall piece, we have simulated the motion of a disk wall, a wall that is surrounded by a string loop, whose thickness is comparable to the size. A collision of a wall and a string-wall which we have surveyed in the previous section is practically a two-dimensional simulation. On the other hand, a full three-dimensional simulation becomes possible in this case. When the computations start, the wall whose radius equals 30 meshes is placed in the $xz-$plane centered on the 128^3 box. Therefore the coordinate of the circular string that encloses the wall is expressed by

$$y = 64\ , \quad (x-64)^2 + (z-64)^2 = 30^2\ . \tag{3.11}$$

The time derivative of χ is zero everywhere in the box. The distribution of V_w at $y = 64$ and $z = 64$ when $t = 0$ is shown in Figures 3.5. At $t = 20\Delta x/c$ it evolves to Figures 3.6. Apparently the size of the wall becomes smaller. It means the energy of the wall has diffused at the periphery and the division to multiple wall pieces is proceeding almost at the light velocity. Such destruction proceeds still more and about 75% of the initial V_w energy has been converted to the $\dot{\chi}$ energy in Figures 3.7 at $t = 40\Delta x/c$. From the viewpoint of the field configuration evolution, it can be said that the false vacuum energy is gradually transferred to the kinetic energy in the course of time.

When string loops decay, it is supposed that they oscillate many times and may radiate gravitational waves[33]. In a spherical collapse, walls actually oscillate a few times[98]. Our simulations, however, do not show any clear oscillation. The reasons are that the initial configuration of previous simulations assumes unreasonable high symmetry which enables bounces; since the spherical wall has no edge, the string tension is ignored; and the wall thickness is much larger than the wall size. The intercommutations and collapses of the walls is so frequent and rapid that there is no enough time for them to make a global motion like fluttering or wriggling.

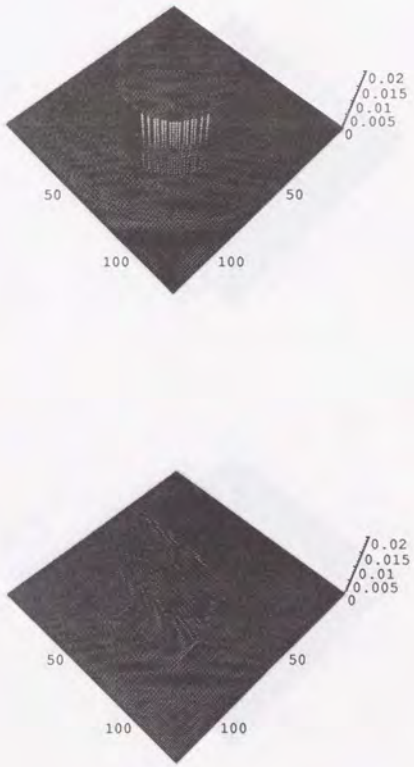

Figure 3.5: Initial V_w potential energy distribution of the disk wall simulation is shown. The upper graph corresponds to the slice $y = 64$, $(x, z) = (1, 1) - (128, 128)$ and the lower one is at $z = 64$, $(x, y) = (1, 1) - (128, 128)$ slice. In this and the subsequent figures, $V_a = 0.01$ and the left-hand-side of the numbered axes is $x-$one in both figures.

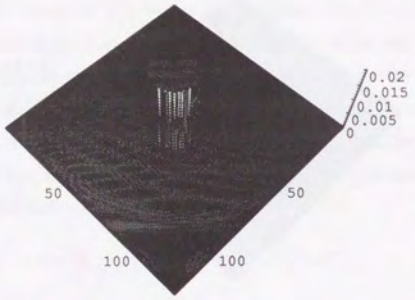

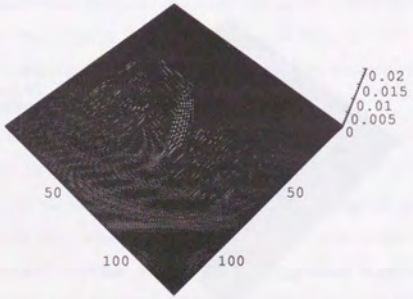

Figure 3.6: After $20\Delta/c$ from the initial configuration is plotted.

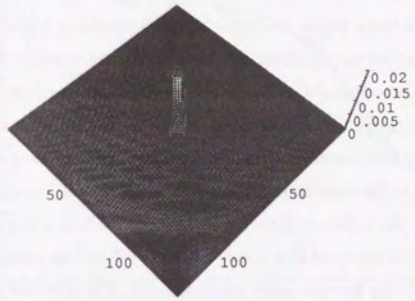

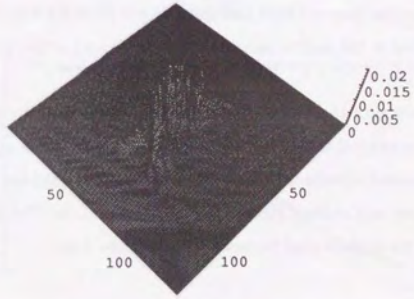

Figure 3.7: After $40\Delta/c$ from the initial configuration is plotted.

3.4 Evolution of Wall Area

Next we look over the time evolution of the wall size in the expanding universe. For this purpose, we have to find a way to determine the total amount of wall area in the simulation box. This can be carried out by counting the number of cells in which the phase of the field, θ_a, takes π, that is, where the false vacuum of V_w remains. However, we can get the value of θ_a only at grid points. Thus it is rather difficult to find out the place at which θ_a equals π exactly. Instead, we have identified sides where the sign of $\sin\theta_a$ changes from plus to minus and yet $\cos\theta_a < 0$ at the same time as the position where walls cross. Using this method, we have calculated the evolution of domain walls numerically in a box who has 100^3 cells.

Initially the amplitude of the field equals v at every cell and the phase is chosen randomly. This corresponds to the thermal phase transition case. The practical change in the initial condition has no effect on the field evolution sufficiently after the stabilizing era. This is because the random motion of the field fluctuation cancels out the initial difference. Of course our following results are deduced from the analysis in this post-stabilization period. Figure 3.8 shows the result in the radiation dominated universe. Evidently the amount of walls has a tendency to decrease with time promptly. Figure 3.9 depicts the case that the expansion law is that in the matter universe. The same trend as the previous figure is also observed here.

Since the resolution of the wall thickness becomes worse with the growth of the scale-factor as we have mentioned these simulations are executed for a few expansion time. Thus the quantitative analysis is limited. However, we can supplement the loss with the qualitative discussion in the previous section. Hence the prediction that the $N = 1$ axion domain wall should not bother the cosmological framework seems to be right.

3.5 Walls as Gravitational Sources

Here we consider one of the cosmic structure formation models. Soft domain walls produced at the late-time phase transition[29] can contribute the cosmological large-scale structures that recent observations have revealed[56, 57]. The term "late-time" means its formation is sufficiently long after the decoupling of matter not to disturb the CMBR and its surface

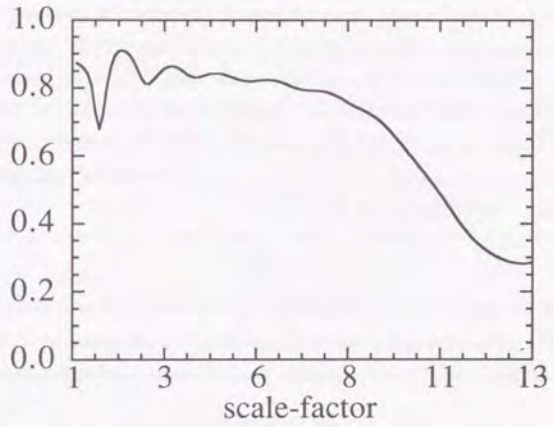

Figure 3.8: This figure shows the evolution of the volume ratio of the cells that contain walls to 100^3, *i.e.*, the number of the total cells in the comoving simulation box. The scale-factor evolves $a \propto \tau$ and is normalized to one at the initial time.

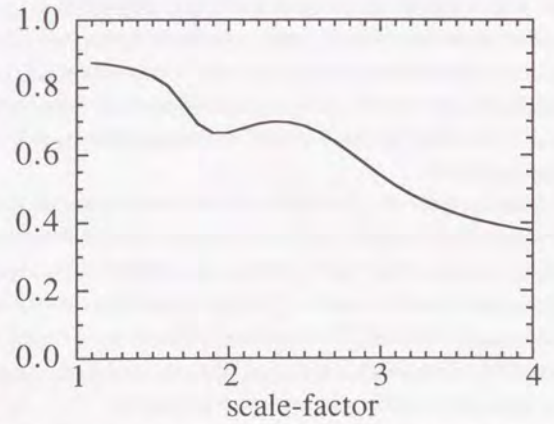

Figure 3.9: The same quantity as Figure 3.1 is plotted but in the matter dominated era.

energy density is small enough not to dominate the universe. For example, the schizon model[99] is one of the actual possibilities. It is a kind of pseudo-Nambu-Goldstone boson, which can be understood as a generalization of the axion. The axion acquires its mass at the QCD scale. In the schizon model, the soft breaking scale of the continuous global symmetry is regarded to be a free parameter. If we suppose this quantity should be a mass scale of a hypothetical fermion, m_f, then the mass of the schizon, m_s, associates with the spontaneously U(1) breaking scale, f_s, as

$$m_s \simeq \frac{m_f^2}{f_s} , \tag{3.12}$$

similarly to the case of the axion in which $m_f \sim$ the QCD scale. If we substitute the GUT scale $\sim 10^{16}$ GeV for f_s and m_f is assumed to be 0.01 eV which is the mass of, for example, a massive neutrino, then the corresponding schizon Compton wavelength is derived as

$$m_s^{-1} \sim 1 \text{ Mpc} , \tag{3.13}$$

which is a cosmologically interesting distance scale. In the model of these parameter, the phase transition occurs at a very low energy scale $\sim$ 0.01 eV. Thus the CMBR is not disturbed significantly by the walls[100]. Moreover, the energy density of the walls is that of the order of the critical density. The schizon wall can be dark matter.

There are several other models of structure formation by domain walls. Cell structure formation may be possible by domain wall networks through the model with an approximate O(N) symmetry[101]. However, in considering these wall models, it is not argued how the walls interact with ordinally matter. The actual mechanism of mass accretion remains to be an unresolved problem.

When we suppose that walls may be seeds of the cosmological large-scale structure, it is important how decaying walls work as gravitational sources. Although it is also argued that walls can sweep up matter with non-gravitational interactions[102], we focus ourselves on the metric perturbations by walls themselves. It is widely believed that a static infinite planar wall acts as a repulsive sheet[103]. The corresponding solution of the Einstein equation is obtained under the approximation that the wall thickness is neglected. Using the energy momentum tensor of the infinitely thin wall pararell to xy-plane :

$$T_{\mu\nu} = \sigma\delta(z)\text{diag}(1,-1,-1,0) , \tag{3.14}$$

the solution of the Einstein equation is found to be :

$$ds^2 = (1-\kappa z)^2 dt^2 - dz^2 - (1-\kappa z)^2 e^{2\kappa t}(dx^2+dy^2) , \quad \kappa \equiv 2\pi G\sigma . \tag{3.15}$$

This is a time-dependent solution. Matter put in this spacetime will be accelerated uniformly to the direction away from the wall, whose magnitude is equal to κ. Hence it can be regarded that the force by the wall is repulsive.

Even in the case that the scalar field is solved exactly, the same argument holds[104]. This can be seen naively considering that the energy-momentum tensor of a scalar field is written as

$$T_{\mu\nu} = \partial_\mu\chi\partial_\nu\chi - \frac{1}{2}g_{\mu\nu}g^{\alpha\beta}\partial_\alpha\chi\partial_\beta\chi + g_{\mu\nu}V(\chi) . \tag{3.16}$$

We can define the energy density, ρ_w, and the mean pressure, p_w, of the field, χ, in the same way as a perfect fluid :

$$\rho_w = \frac{1}{2a^2}\dot{\chi}^2 + \frac{1}{2a^2}(\nabla\chi)^2 + V(\chi) , \tag{3.17}$$

$$p_w = \frac{1}{2a^2}\dot{\chi}^2 - \frac{1}{6a^2}(\nabla\chi)^2 - V(\chi) . \tag{3.18}$$

For a static wall, the time-derivative of χ equals zero and the potential energy should be positive where the false vacuum is left behind. Thus when the wall is not moving, it acts as matter of negative pressure analogous to the cosmological constant.

In general, the amplitude of the gravitational effect by a scalar field is evaluated by the sum of the diagonal elements of the energy-momentum tensor which plays a role of the source for the growth of the linear matter perturbation[105]. In order to evaluate the linear metric perturbation, we decompose the spacetime metric as

$$g_{\mu\nu} = a(\tau)^2[\eta_{\mu\nu} + h_{\mu\nu}] , \tag{3.19}$$

under the synchronous gauge; $h_{0\nu} = 0$. Here we substitute $\text{diag}(1,-1,-1,-1)$ for $\eta_{\mu\nu}$. Hence the unperturbed background spacetime is Minkowskian. Then one of the Einstein equations reads

$$-\ddot{h} - \frac{\dot{a}}{a}\dot{h} = 3\frac{\dot{a}^2}{a^2}\delta + 8\pi\sum_\mu T_{\mu\mu} , \tag{3.20}$$

where δ is the density perturbation in pressureless matter which is related to $h \equiv h_{11} + h_{22} + h_{33}$ as

$$\dot{\delta} = -\frac{\dot{h}}{2} . \tag{3.21}$$

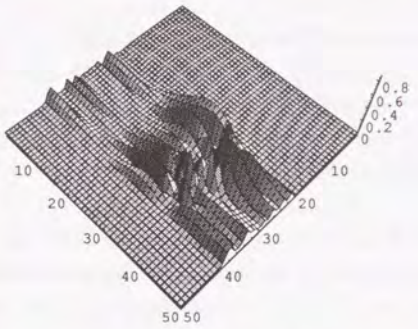

Figure 3.10: Distribution of the gravitational source density, S_χ, at the same time and space as Figure 3.2 is demonstrated. Here $V_a = 0.01$ and $\lambda v^4 = 1$.

Therefore we can identify the second term in the right-hand-side of the equation (3.20) as an effective mass density for the metric perturbations. Using the Minkowski metric as $g_{\mu\nu}$ in the equation (3.16), the gravitational source density, S_χ, can be defined as

$$S_\chi \equiv 2\dot{\chi}^2 - 2V(\chi) \ . \tag{3.22}$$

When the field configuration is static, $\dot{\chi} = 0$. Thus in the region of the false vacuum where the potential term is nonzero, S_χ is negative and the repulsive force is expected for a motionless wall.

Since we have the original field configuration, we can calculate the gravitational source density, S_χ, for the interacting walls directly. This quantity is plotted in Figure 3.10 at the same time and slice in Figure 3.2. The peak of S_χ approximately indicates the place of the string that is moving at high velocity ($\sim 0.5c$). On the whole S_χ is positive in the region where the phase of the field changes greatly. Also in the situation in the subsection 3.3.2, we have calculated the distribution of the gravitational source. The fact that the source density is positive in the wall interacting region where the wall is shrinking into is verified

as well. Thus the intercommuting or contracting wall operates as a seed of attractive force. Unlike a simple static wall whose gravitational force is repulsive, moving walls are quite normal gravitational sources.

3.6 Summary

We have investigated the dynamics of the scalar field that obeys a potential in the equation (3.3). When the field settles into a true vacuum, a connected string-wall system develops. The subsequent motion of the hybrid topological defects has been understood. The simulation scheme is different from those by Press et al.[106], Kawano[107] and Ryden et al.[94] in the fact that we have treated an isolated system well within the horizon scale although they followed the evolution of super-horizon walls whose shape is complex and irregular. Our simulations have been performed in two-dimensional or three-dimensional space, thereby they are much more realistic than those by Widrow[98] in which the walls has no string edge.

When the number of wall joined to the string is only one, such walls dissipate the energy at the speed of several tens of percent of the light velocity and finally are annihilated, although this process is slowed down by the expansion of the universe. Thus the $N = 1$ domain wall does not contradict the observation of our universe. It gives a unique valid axion model, which confirms the previous view.

It is remarkable that the interactions between walls are very violent. The oscillations of the wall pieces are hardly observed in contrast to the simple string loop without a wall[33]. It indicates that the false vacuum energy of domain walls is released mainly by a scalar field mode rather than by gravitational waves, although there exists a possibility that the walls lose their energy through the non-gravitational interactions[108]. Such a situation may be also appeared in the case of pure strings. The conventional analysis is rough estimation; the energy loss rate by gravitational radiation $\sim G\mu^2$, the frequency of them is a reciprocal of loop size. Whether they are true or not should be committed to further study.

The gravitational source density has been calculated from the field configuration in two cases, intercommuting walls and a small wall piece. Both results show that the interacting walls generate positive gravitational energy and produce attractive gravitational force. Such

non-Gaussian seeds may help the scenario of the large-scale structure formation by the domain walls. It is an important disagreement against an infinite static wall[103, 104].

Chapter 4

Global Textures

The dynamical evolution of global textures is studied in the present chapter. The evolution equation of a texture field is solved numerically and the effects of cosmic expansion and radial motion are explicitly incorporated. The process of knot collapse is traced and the density perturbations by textures are investigated by a cluster analysis. High density clusters posses large-scale correlation and extend widely, which may be useful for the formation of large-scale structure. However, it is shown that, although they obey non-Gaussian statistics and a hierarchical behavior is achieved in the linear regime, galactic-scale fluctuations are practically Gaussian initially. Hence the texture model should be no better than the standard Gaussian model.

4.1 One Texture in the Whole Universe

Global textures are topological defects which are produced at phase transitions accompanied by a certain class of symmetry breaking through the so-called Kibble mechanism or some kinds of non-thermal phase transitions. They come into existence when the third homotopy group of the true vacuum manifold is non-trivial. For example, the family symmetry model has a global SU(2) symmetry[109] and global textures arise when this symmetry becomes broken.

Textures are essentially different from other defects, such as domain walls or cosmic strings, in that they are topologically unstable. After the phase transition, each point in the universe settles down in some true vacuum state. They hold their energy as a field gradient

not as a false vacuum energy.

As a demonstrative example of the cosmological importance of a texture, here we briefly introduce the case that one global texture exists in a closed universe[110]. When the global symmetry breaking such as O(4)→O(3) occurs, the vacuum structure is written by $\pi_3(\mathrm{O}(4)/\mathrm{O}(3)) = \mathbf{Z}$, which enables the existence of textures.

In the first place, we rewrite the metric of the closed spacetime, the equation (1.1) when $k = 1$, as

$$\begin{aligned} ds^2 &= dt^2 - a^2(t)\left[d\eta^2 + \sin^2\eta(d\theta^2 + \sin^2\theta d\varphi^2)\right] \\ &\qquad (0 \le \eta \le \pi,\ 0 \le \theta \le \pi,\ 0 \le \varphi \le 2\pi)\ . \end{aligned} \tag{4.1}$$

After the phase transition, when the condition $|\chi| = v$ holds, a stable texture exists due to the positive curvature of the spacetime. The solution whose winding number equals one is written by

$$\begin{aligned} \chi = v &\begin{pmatrix} \cos\varphi\sin\theta\sin\left(\frac{\eta}{\varepsilon}\right) \\ \sin\varphi\sin\theta\sin\left(\frac{\eta}{\varepsilon}\right) \\ \cos\theta\sin\left(\frac{\eta}{\varepsilon}\right) \\ \cos\left(\frac{\eta}{\varepsilon}\right) \end{pmatrix} \qquad 0 < \eta \le \varepsilon\pi\ , \\ &= \begin{pmatrix} 0 \\ 0 \\ 0 \\ v \end{pmatrix} \qquad \varepsilon\pi < \eta \le \pi\ , \end{aligned} \tag{4.2}$$

where $0 \le \varepsilon \le 1$. The total gradient energy, E_t, which this texture solution has is

$$\begin{aligned} E_t &\equiv \frac{1}{2}\int(\partial_i\chi)^2 d^3x \\ &= 2\pi v^2 a(t)\left[\frac{\pi}{2\varepsilon} - \frac{1}{4\varepsilon^2}\sin 2\varepsilon\pi + \varepsilon\pi\right]\ . \end{aligned} \tag{4.3}$$

In two limits of opposite directions, E_t approaches the values :

$$\begin{aligned} E_t &\propto \varepsilon && ;\ \varepsilon \longrightarrow 0\ , \\ &\propto [1 + (1-\varepsilon^2)^2 + \cdots] && ;\ \varepsilon \longrightarrow 1\ . \end{aligned} \tag{4.4}$$

When $\varepsilon \to 0$, E_t takes the minimum energy at $\varepsilon = 0$. On the other hand, E_t decreases also in the limit $\varepsilon \to 1$. Hence somewhere in the region $0 \le \varepsilon \le 1$, there should exist an

maximum energy point. In favor of this energy barrier, a stable global texture configuration is realized at $\varepsilon = 1$. The corresponding energy momentum tensor is

$$T_{\mu\nu} = \frac{v^2}{2a^2(t)}\mathrm{diag}(-3,-1,-1,-1)\ . \tag{4.5}$$

Then the energy density of this texture, ρ_t :

$$\rho_t = \frac{3v^2}{2a^2(t)}\ , \tag{4.6}$$

and its pressure, p_t :

$$p_t = -\frac{1}{3}\rho_t\ , \tag{4.7}$$

are deduced. Including the texture energy density, the Einstein equation (1.4) is rewriten as

$$\frac{1-\gamma}{a^2(t)} = (\Omega - 1)H^2\ , \qquad \gamma \equiv 4\pi G v^2\ . \tag{4.8}$$

Thus even when the density parameter of the actual universe surpasses 1, the apparent energy density of the ordinary matter can be estimated to be less than ρ_{cr}. That is, a closed universe can be observed by the dynamical estimation of the amount of matter as a flat or open one owing to the existence of a texture. For the universe to be flat, it is necessary $v \sim M_{pl}$, *i.e.*, the texture producing phase transition should take place at the Planck scale.

Another interesting implication of the stable texture is that it may resolve the horizon problem [111]. Since the universe is closed, the photons of CMBR we observe today could be released within the horizon at the decoupling time. For instance, in the case that $\gamma = 1$ and $\Omega_0 = 1$, the constraint to the present scale of the universe is

$$\frac{5.9}{h} \lesssim \frac{a_0}{3\times 10^2\ \mathrm{Mpc}} \lesssim \frac{6.2}{h}\ , \tag{4.9}$$

where a_0 is defined by the normalization, $k = 1$. The isotropy of CMBR keeps on during the time :

$$\Delta t \approx \frac{0.4\times 10^9}{h}\ \mathrm{year}\ . \tag{4.10}$$

The duration time, Δt, and the permitted range of a_0 are not much affected unless the parameters(Γ or Ω_0) are not unreasonably altered.

4.2 Overview of the Cosmological Textures

The global texture model has been considered to provide a potentially favorable scenario for large-scale structure formation among many candidates, since textures in typical grand-unification scales produce density fluctuations having a reasonable amplitude with a scale-invariant spectrum[40, 112, 43]. The statistics of the fluctuations in this model have been shown to obey a positively skewed non-Gaussian distribution[113, 43], and it has been advocated that, thanks to this property, the texture model predicts early star- and galaxy-formation compared with the standard Gaussian CDM model[114]. After Albrecht and Stebbins[115] have proposed that cosmic strings result in more Gaussian perturbations than was previously supposed, textures become increasingly appealing as origin of conspicuous inhomogeneities.

As unstable topological defects, textures vanish by liberating their energy. When the event horizon extends enough along with the cosmic evolution, the configuration of the Higgs field becomes homogeneous and the spatial differential energy of textures concentrates and the gradient energy is confined to a smaller region at the speed of light. This energy concentration is called a knot. In succession, when the gradient of the field comes to be larger than a potential barrier, knots disappear with a phase jump and a topologically trivial configuration is realized. As a result, the field sits on the same point in the vacuum manifold everywhere. This process is called unwinding of knots[116]. Knots are something like cores of textures and their dynamical evolution perturbs the metric of the universe[117] so that matter is re-distributed to form galaxies or clusters of galaxies. Knots act on the matter like point seeds. Then the induced fluctuations should yield a non-Gaussian form. If the unwinding rate of knots is constant in time, the spectrum of their distribution is scale-invariant. The matter density fluctuations caused by knot collapse should also be scale-invariant and can be useful sources of the large-scale structures of the universe. In addition to the such point-like seeds, a pancake-like accretion pattern can be formed by toroidal symmetric global textures[118].

To investigate the evolution of a texture field, Spergel *et al.*[119] solved the evolution equation numerically and showed that the texture obeys the scaling solution. They also calculated the knot unwinding rate per horizon volume per horizon time; their result shows

that this rate is constant. They, however, modified the equation so that the effect of cosmic expansion on the potential term was neglected. In the subsequent sections, we use an original and unmodified equation to see how this scaling of potential affects the knot unwinding rate.

With the intention of sketching a typical knot collapse we employ a real scalar field χ^j that consists of four components ($j = 1, \ldots, 4$) with the following Lagrangian :

$$\mathcal{L} = \frac{1}{2}(\partial_\mu \chi^j)(\partial^\mu \chi^j) - V(\chi) \ , \quad V(\chi) = \frac{\lambda}{4}(\chi^j \chi^j - v^2)^2 \ , \tag{4.11}$$

where repeated indices implicitly denote a summation. Since there is no false vacuum region in the texture configuration, the field strength can be restricted to the symmetry breaking scale. Under the assumption that $\chi^j \chi^j = v^2$, the field equation is derived as

$$\nabla^\mu \nabla_\mu \chi^j = -\frac{\nabla^\mu \chi^j \nabla_\mu \chi^j}{v^2} \chi^j \ , \tag{4.12}$$

where ∇^μ represents a derivative operator. Assuming a spherically symmetric configuration :

$$\chi^j = v \begin{pmatrix} \cos\chi_0 \\ \sin\chi_0 \sin\theta \cos\varphi \\ \sin\chi_0 \sin\theta \sin\varphi \\ \sin\chi_0 \cos\theta \end{pmatrix} \ , \tag{4.13}$$

where θ and φ are the coordinate components of polar angles, the degree of freedom is reduced to only one valuable, χ_0. Then the evolution equation (4.12) reads

$$\ddot{\chi_0} - \frac{2}{r}\frac{d\chi_0}{dr} - \frac{d^2\chi_0}{dr^2} = -\frac{\sin(2\chi_0)}{r^2} \ , \tag{4.14}$$

in a flat Minkowski spacetime.

For the texture of unit unwinding number, the collapsing solution exists :

$$\chi_0 = \begin{cases} 2\tan^{-1}\left(-\dfrac{r}{t}\right) \ , & t < 0 \ , \\ 2\tan^{-1}\left(\dfrac{r}{t} + \pi\right) \ , & t > 0; \ r < t \ , \\ 2\tan^{-1}\left(\dfrac{t}{r} + \pi\right) \ , & t > 0; \ r > t \ , \end{cases} \tag{4.15}$$

in which χ_0 changes from 0 at $r = 0$ to π at $r = +\infty$ when $t \to -\infty$ and is always equal to π when $t \to +\infty$. Thus the unwinding of a texture knot is realized. With equation (3.16) the energy momentum tensor for this solution can be calculated and the metric perturbation

can also be expressed using the Einstein equation. As a result, under the approximation that the photon emission occurs at infinite past and it is received at infinite future, the temperature distortion by the Sachs-Wolfe effect results in :

$$\frac{\delta T}{T} = 8\pi^2 G v^2 \frac{t_c}{(2r_c^2 + t_c^2)^{1/2}} , \tag{4.16}$$

where r_c is the impact parameter for the photon path to the knot center and t_c denotes time measured from the texture collapse. The maximum temperature fluctuation is realized when $r_c = 0$ but its sign depends on whether t_c is positive or negative. When the light ray goes through the nearest access point after the knot collapse, *i.e.*, $t_c > 0$, the travelling photon is blueshifted and a hot spot will be observed on the sky. In the contrary case, a redshifted cold spot should be discovered. With the aid of numerical results, Spergel *et al.*[119] predicted that about 10 spots of angular radius $\sim 8^\circ$ should be contained in the CMBR assuming the universe has been fully reionized. In the section 4.4, it is shown that this is an overestimated number.

The recent COBE observation detected the root-mean-square temperature fluctuations at 10° cited in the equation (1.10). This scale corresponds to the horizon of the last scattering surface in the reionized universe. If we apply the above scenario, the result of COBE may put a stringent restriction on textures by counting hot and cold spots, which is difficult due to the lack of resolution. Moreover, the COBE result indicates that the reionization model, which itself is realized in limited situations, is less preferable than the standard one[120]. Although as for the absolute temperature fluctuations, the exact value which the texture model predicts depends on the details of the model, it turns out to be consistent with the COBE observation by taking the bias parameter to be $b \approx 2 - 3$[121, 122]. In addition to the CMBR bumps by simple spots model, the anisotropy from scalar field gradient also predicts the grand unified scale texture[123]. Thus global textures cannot be fully excluded by the CMBR observation.

Gooding *et al.*[41] and Cen *et al.*[42] investigated the plausibility of texture-seeded universe scenarios, both textures with CDM and those with HDM. They made use of hydrodynamical simulations. Their main conclusions are that galaxies and clusters of galaxies have correlations of significantly larger scales than those in the models without textures, and that the early formation of these objects are highly promoted. Above favorable features of the

texture cosmology must originate from the non-Gaussian nature of them. Abundant sticking density peaks will enhance matter accretion. These simulations, however, are based on the initial texture fluctuations calculated by Spergel *et al.*[119], in which the basic equation was improperly deformed. Thus we pay careful attention to how strong the texture model exhibits a non-Gaussian disturbance in the section 4.6 using the correct equation.

4.3 Numerical Scheme

In simulations we consider the simplest global texture model, G=O(4) and H=O(3), in which the production of global textures is possible. We use the Lagrangian given by equation (4.11). The spatially-flat Friedmann-Robertson-Walker metric (2.9) is assigned to the unperturbed background. In this background spacetime, we solved numerically the field equations for χ^j :

$$\frac{\partial^2 \chi^j}{\partial \tau^2} + \frac{2}{a}\frac{da}{d\tau}\frac{\partial \chi^j}{\partial \tau} - \nabla^2 \chi^j = -a^2 \frac{\partial V}{\partial \chi^j} , \tag{4.17}$$

in a three-dimensional comoving cubic box, which is identical to the equation (3.9) in the wall-string situation. The values of four components for χ are allocated to each lattice point.

In the process of solving the equation (4.17) numerically, a discretization method has been employed. The equations are expressed by

$$\begin{aligned} &\frac{\dot{\chi}^{n+1}_{x,y,z} - 2\dot{\chi}^{n}_{x,y,z} + \dot{\chi}^{n-1}_{x,y,z}}{\Delta\tau^2} + 2\frac{\dot{a}}{a}\frac{\dot{\chi}^{n+1}_{x,y,z} - \dot{\chi}^{n-1}_{x,y,z}}{2\Delta\tau} \\ &- \frac{\chi^{n}_{x+1,y,z} - 2\chi^{n}_{x,y,z} + \chi^{n}_{x-1,y,z}}{\Delta x^2} - \frac{\chi^{n}_{x,y+1,z} - 2\chi^{n}_{x,y,z} + \chi^{n}_{x,y-1,z}}{\Delta y^2} - \frac{\chi^{n}_{x,y,z+1} - 2\chi^{n}_{x,y,z} + \chi^{n}_{x,y,z-1}}{\Delta z^2} \\ &= -a^2 \lambda \chi^{n}_{av}\left(|\chi^{n}_{av}|^2 - v^2\right) , \end{aligned} \tag{4.18}$$

$$\chi^{n}_{av} \equiv \frac{1}{6}\left(\chi^{n}_{x+1,y,z} + \chi^{n}_{x-1,y,z} + \chi^{n}_{x,y+1,z} + \chi^{n}_{x,y-1,z} + \chi^{n}_{x,y,z+1} + \chi^{n}_{x,y,z-1}\right) , \tag{4.19}$$

where an upper suffix denotes the number of time steps and a lower suffix shows a spatial coordinate in a simulation box. We set the lattice spacing equal to 1, that is, $\Delta x = \Delta y = \Delta z = 1$ in simulations. A conformal time step is selected so as to satisfy the Courant condition[87].

Numerical calculations are performed in the cube of $\leq 100^3$ mesh points with a periodic boundary condition. The initial condition is designed as follows. The initial comoving lattice interval was chosen so as to coincide with the initial horizon length. Thus χ at each

point should have a random value since there is no causal relation over a unit cell under the thermal phase transition. Initial values of χ^1, χ^2, χ^3 and χ^4 are determined randomly under the restriction $\chi^j\chi^j = v^2$ and $\dot{\chi}^j = 0$. In the quantum phase transition case, the phase correlations according to the equation (2.65) should be included, which would reduce the number density of defects. Finally, we took $\lambda = 0.04$ or 0.01 as reasonable values of coupling constant, and $v = 1$; all the scales are normalized by the value of v.

We have performed several test runs in which other values of parameters are adopted or the initial condition is altered. The results of these simulations give no essential discrepancy to our conclusion. Particularly the simulations of the false vacuum initial condition, *i.e.*, $\chi = 0$ differ only in the initial temporary behavior of the stabilizing process from those of the true vacuum initial condition we have employed. We have also confirmed that there is no finite volume effect by comparing the results of the different box sizes.

In the sections 4.4 and 4.5, we have done calculations using two expansion laws of the extreme cases. One is that in the radiation dominated universe. Hence the scale-factor depends on the conformal time such as $a(\tau) \propto \tau$. The other is for the matter dominated universe, that is, $a(\tau) \propto \tau^2$. On the other hand, the era in the vicinity of the equality time is treated in the section 4.6. Hence more realistic formula is adopted; τ and $a(\tau)$ are related to each other as $\tau \propto \sqrt{a + a_{eq}} - \sqrt{a_{eq}}$. Then we followed the evolution until the horizon scale became larger than about forty meshes. The system relaxed into the scaling solution before five expansion times when the behavior of the field became independent of the details of the initial condition, and we start collecting data to analyze the statistical properties.

To investigate the evolution of a texture field, a modified equation in which the effect of cosmic expansion was completely taken into account has been used in the paper by Spergel *et al.*[119]. Furthermore, Pen *et al.*[122] fixed $\chi^j\chi^j = v^2$ throughout the calculations, neglecting the radial-mode fluctuations. However, the field oscillates around the true vacuum, not only along the massless Goldstone mode, but also along the radial direction; the perturbations due to these processes are also important in the texture model. We thus used the precise equation (4.17), in which both cosmic expansion and radial fluctuations are fully considered.

4.4 Knot Collapses

In this section, we estimate the knot unwinding rate numerically and verify the scale-invariance of knot collapses. We define the knot number per horizon volume at the moment of the phase transition, N_k. As the horizon expands, knots are formed continuously. Thus if knots were stable, the knot number per horizon volume would be $N_k\tau^3$. However, knot collapses at the speed of light. On the other hand, the horizon scale evolves also at the speed of light. By naive consideration, we can presume that the knot number per horizon volume should take the constant value, N_k. The knot number per comoving volume, n_k, is written by

$$n_k = \frac{N_k}{\tau^3}. \tag{4.20}$$

To determine the value of N_k, we searched for a knot point in the simulation box. For the purpose of the direct determination of a texture's position, the phases of χ are evaluated at the central point of each cell. At all sides of each cell, it is checked if the sign of the χ field changes. The cells which have the side where all the components of χ changes their signs are counted for topological singularity, since the field should sit on the false vacuum somewhere in this cell. The time evolution of the number of these cells is shown in Figure 4.1 and 4.2, where we set λ as 0.04. Then the enough resolution for knots counting is ensured. In Figure 4.1, the expansion law is that in the radiation dominated universe. Figure 4.2 is for the matter dominated universe. In both cases, the estimation of N_k starts well after the field settles in the true vacuum and stops well before the computation fails. The former figure shows $N_k \sim 0.01$ and the latter shows $N_k \sim 0.02$. These results demonstrate the constancy of the knot unwinding rate per horizon scale.

Using geometrical considerations, Prokopec[124] calculated the probability for the formation of texture per correlation volume, which equals the horizon volume in our simulations, to be $0.01 \sim 0.21$. His method of estimation is based on the Kibble mechanism. Space is divided to simplexes and five tetrahedra, the central one and the four adjacents ones which own single face in common with the first one are imagined. Then the probability of the events that the winding number around them exceeds critical value, n_c, can be computed by geometrical estimation. The biggest value, 0.21, is gained when $n_c = 0.5$ and the smallest one, 0.01, corresponds to the case $n_c = 1$. The numerical value is consistent with that of

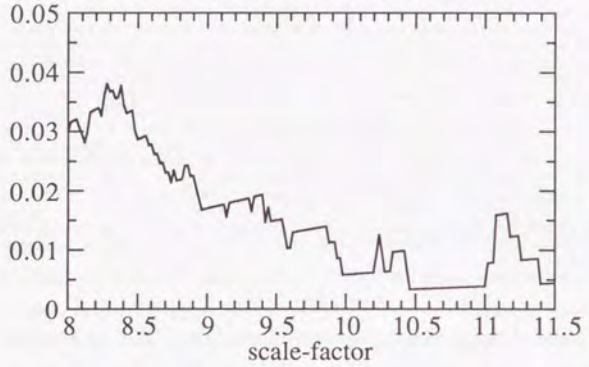

Figure 4.1: The time evolution of the knot number per horizon volume is shown. $\lambda = 0.04$ and the scale-factor grows with $a(\tau) \propto \tau$. The knot unwinding rate is almost constant in time. N_k in the equation (4.23) is about 0.01.

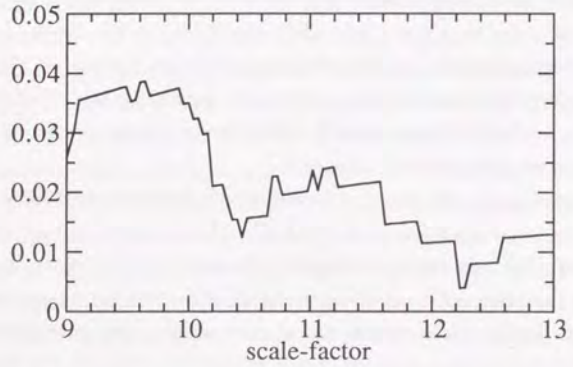

Figure 4.2: The same as the previous figure is shown in the case where $\lambda = 0.04$ and $a(\tau) \propto \tau^2$. $N_k \sim 0.02$ in the matter dominated universe.

Monte Carlo simulations[125]. Our results agree with this value. The result implies that the field configuration which enables topological defects is rarely realized; its probability is much smaller than unity.

Thus we can say that the value of N_k is $0.01 \sim 0.02$, which is smaller than that obtained by Spergel *et al.*[119]. They identified grid points where the magnitude of χ is large enough as texture unwinding points. Probably this is one of the reasons why they overestimated the knot unwinding rate. Our definition of knots picks up only the point where the winding number exceeds ~ 1. Their criterion, $|\chi| < v/2$, is too crude.

4.5 Distribution of Density Peaks

It is important to investigate the distribution of an effective mass density produced by the texture field, χ, for the purpose of studying the structure formation of the universe. The fact that $N_k \ll 1$ indicates that the knot unwinding does not happen so frequently. Global textures, however, always give perturbations to the mass density of the universe throughout their dynamical evolution. There is also an differential energy concentration where a knot collapse does not occur, since the process of the χ configuration developing into a uniform phase state within the horizon scale proceeds continually. We can get the information about how textures disturb the matter density by examining the spatial distribution of the gravitational source density.

In this section, we concentrate on the case where $\lambda = 0.01$ and $a(\tau) \propto \tau$ as a typical one. Simulations under any other reasonable parameters also show the common conclusions with the above case. Figure 4.3 shows the time evolution of the gravitational source density, S_χ defined in the equation (3.22). After the initial stabilizing era, the averaged gravitational source density over the simulation box decreases with an oscillation. The rate of decrease is $\propto a^{-3}$, which is consistent with the behavior of the scalar field in an expanding universe. The oscillation is caused by the wandering of the Higgs field around the potential minimum in a radial mode. Hence the frequency is $\sim \sqrt{\lambda v^2}$ in proper time. This time evolution indicates the importance of the mass of χ. Thus the approximation by Pen *et al.*[122] that the height of $V(\chi)$ has no influence on the evolution of χ is inadequate.

To investigate the perturbations by textures, we should pay attention to high S_χ peaks

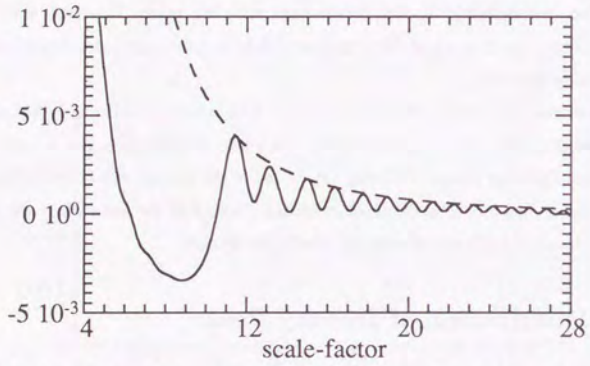

Figure 4.3: The gravitational source density, S_χ, evolution is depicted. The unit of the vertical axis is normalized by v^4. The parameter, λ, equals 0.01. The scale-factor evolves in the same manner as that in a radiation dominated universe. The dashed line is the power-law fitting line of the peak of S_χ. The index of this line equals -3.

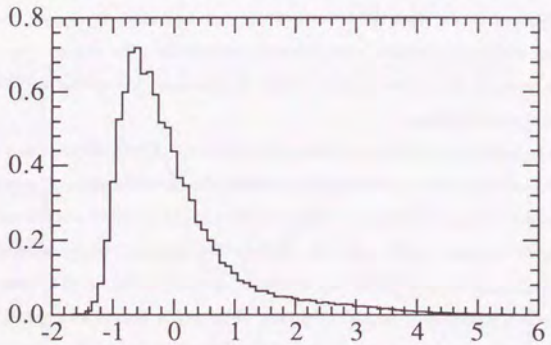

Figure 4.4: The statistical distribution of the gravitational source density, S_χ, at $a = 14.12$ of the simulation in which $\lambda = 0.01$ and $a(\tau) \propto \tau$ is shown. The horizontal axis is rescaled so that the dispersion is equal to unity. The vertical axis is the probability. The value of σ_S is 0.0015.

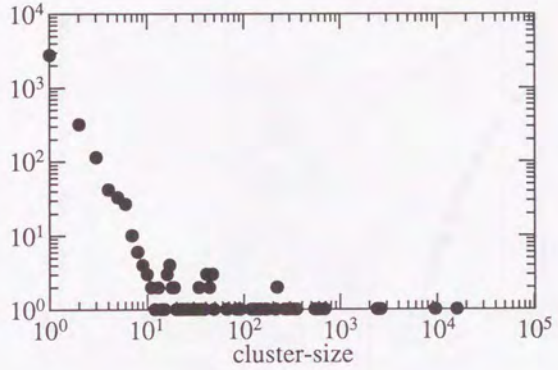

Figure 4.5: This figure exhibits the high density cluster distribution at $a = 14.12$. The parameters in the simulation are common with that of Figure 4.4. The horizontal axis shows the cluster size and the vertical axis shows its number. The threshold equals $\bar{S}_\chi + \sigma_S$.

and its spatial distribution rather than the property of an averaged quantity. First, we calculate the statistical distribution of S_χ at a certain time slice. Figure 4.4 shows that the density distribution by textures is highly non-Gaussian and has a long high density tail. This suggests that the mass irregularities are formed promptly, which should be completely different from the density fluctuation growth in a Gaussian model. The moment that the distribution skews negatively, however, also exists in the texture evolution. Hence the statistics of perturbations by textures are not so simple and need to be studied further.

To express the spatial density distribution more qualitatively, we have used a clustering analysis. First the threshold density is defined; if the gravitational source density at a certain cell is larger than the value of the threshold, we regard it as a high density cell. Then all the linked neighboring high density cells are assumed to be members of "cluster". Then the spatial distribution of the gravitational source is exhibited by examining the size-number distribution in a three-dimensional box. Figure 4.5 describes the result when the threshold equals $\bar{S}_\chi + \sigma_S$, where $\bar{S}_\chi$ is the mean of S_χ over the simulation box and σ_S is the dispersion of S_χ. For comparison, the result of the same analysis in the case where the

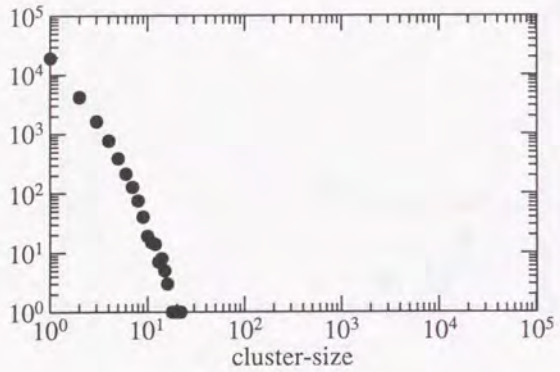

Figure 4.6: This is calculated from the configuration where the high S_χ points whose number is equal to that in the previous figure are distributed randomly.

high density cells are distributed at random is shown in Figure 4.6, whose profile differs from that of the texture simulation. Evidently high density peaks by global textures are strongly correlated since the former distribution has much larger clusters than the random simulation. Particularly the existence of the cluster whose size is extremely large indicates the wall-like or string-like structure by the texture perturbations. To see the correlation of S_χ explicitly, the three-dimensional distribution is demonstrated in Figure 4.7. A dotted point corresponds to the cell where the gravitational source density exceeds $\bar{S}_\chi + \sigma_S$. It is obvious that large-scale clusters exist, which is quite different from Figure 4.8 in which dotted cells are randomly distributed.

We have calculated S_χ cluster distribution at various time slices. The profile is time independent and the following statement always holds even when the scale-factor is greater than 20. Since the horizon scale τ equals 20 at $a = 20$, there is only one or no knot in a 70^3 box at this time if $N_k \sim 0.01$. In spite of the scarcity of knots, the spatial distribution of high density peaks looks very similar. Hence the texture evolution is scale-invariant in the sense that the size distribution of density peaks holds unchanged. This is in good agreement with the scale-invariance of knot collapses. Of course we must follow the evolution of density

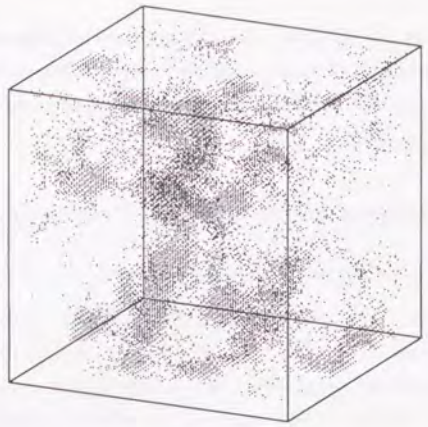

Figure 4.7: The three-dimensional distribution of the high density cells in a 50^3 box at $a = 13$ is shown. Dotted cells correspond to the cell where $S_\chi \geq \bar{S}_\chi + \sigma_S$.

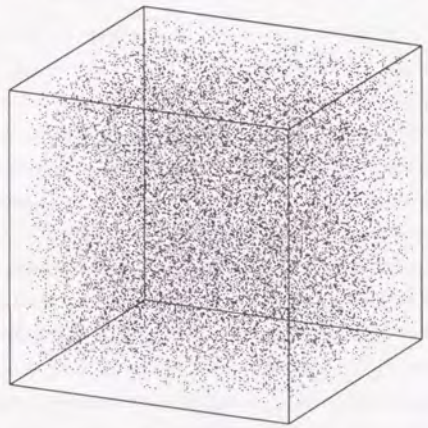

Figure 4.8: Dotted cells are randomly distributed such that the total dotted volume is identical to that of the previous figure.

fluctuations to compare the texture density distribution with the observed structure in our universe. However, the statistical property of the perturbations by global texture itself is noteworthy. Global textures may offer a mechanism of producing the correlated mass distribution in the universe.

4.6 Analysis of the Statistical Properties

4.6.1 Formulation of the Method

In the present section, we analyze the statistical properties of density perturbations by global textures making use of the results of numerical simulations in the previous sections[126]. Observationally, the existence of highly non-Gaussian distribution of galaxies is known at present[58]. The observed reduced three- and four-point correlation functions have been shown to satisfy a hierarchical form[127, 128] which can be expressed in terms of their volume average as

$$\overline{\zeta}(V) = S\overline{\xi}^2(V) \ , \qquad \overline{\eta}(V) = K\overline{\xi}^3(V) \ , \tag{4.21}$$

where $\overline{\xi}(V)$, $\overline{\zeta}(V)$, and $\overline{\eta}(V)$ are two-, three-, and four-point reduced correlation functions averaged over volume V, respectively, with S and K being constants which are independent of V. Although there have been some attempts to explain its origin in some limited situations[129, 130], it is yet unclear how this hierarchy is realized on various scales. It may be explained by a nonlinear gravitational interaction[131] and/or by a non-Gaussian initial condition. We furthermore discuss the prediction of texture-seeded perturbations in relation to these higher-order correlation functions.

In the section 4.3, we have calculated the knot distribution aspect. However, the point-like view of the fluctuations is too simple to be applied to a statistical analysis. We have evaluated the knot number per horizon volume to be $0.01 - 0.02$ with the aid of numerical calculations. Although knot collapse is such a very rare process, textures can perturb the matter distribution, even outside of the region where the knots unwind. This is because the unwinding occurs only when the winding number becomes close to unity, whereas a phase rearrangement always occurs everywhere in the universe, since the horizon spreads continuously. We thus employ the spatial distribution of the texture field in order to check

the statistics of perturbations by textures.

In the same manner as the equation (3.22), the quantity corresponding to the gravitational source of the scalar field is expressed by the sum of diagonal parts in the energy momentum tensor, namely :

$$S_\chi(t,\mathbf{x}) \equiv 2\dot{\chi}^j\dot{\chi}^j - 2V(\chi) \ , \tag{4.22}$$

where a dot denotes a derivative with respect to time t. Then the normalized density perturbation of matter, $\delta(t,\mathbf{x}) \equiv (\rho_m(t,\mathbf{x}) - \bar{\rho}_m(t))/\bar{\rho}_m(t)$, evolves with time in the linear regime when there is no drag force between matter and radiation, following the linear perturbation equation[127] :

$$\ddot{\delta} + 2\frac{\dot{a}}{a}\dot{\delta} = 4\pi G\left(\bar{\rho}_m\delta + \Delta S_\chi\right), \tag{4.23}$$

where $\Delta S_\chi(t,\mathbf{x}) \equiv S_\chi(t,\mathbf{x}) - \bar{S}_\chi(t)$. $\rho_m(t,\mathbf{x})$ is the matter energy density at $(t,\mathbf{x})$; $\bar{\rho}_m(t)$ and $\bar{S}_\chi(t)$ are the spatial average of $\rho_m(t,\mathbf{x})$ and $S_\chi(t,\mathbf{x})$. Since we know the two independent solutions for the equation without the ΔS_χ term[127], we can write the solution of equation (4.23) for the growing mode as

$$\delta = \frac{6\pi G}{\rho_{eq}}\left(1+\frac{3}{2}a\right)\int_{a_i}^{a} da'\Delta S_\chi\frac{a'^3}{1+a'^2}\left[\left(1+\frac{3}{2}a'\right)\sqrt{1+a'}\log\frac{\sqrt{1+a'}+1}{\sqrt{1+a'}-1} - 3\left(1+a'\right)\right] \ , \tag{4.24}$$

where ρ_{eq} is the matter density at $a = a_{eq}$, and we have set $\delta = \dot{\delta} = 0$ at $a = a_i$. The amplitude of fluctuations was properly normalized according to the observation by taking the biasing parameter to be 2[121].

When we evaluated S and K, we calculated the evolution of δ, with $a_{eq} = 1$ and $a_i = 0.2$, starting the simulation at $a = 0.02$ and confirming that the system had already settled into the scaling regime by the time $a = a_i$. Since our primary purpose is to investigate the statistical properties of the initial condition before the nonlinear gravitational interaction deforms them, we should analyze the distribution of $\delta(t,\mathbf{x})$ at some early epoch. It would be most appropriate to do so at the equality time, since the largest structures observed today are supposed to have been seeded by a texture collapsing around this time[112], and clustering of matter should have become effective at that time.

4.6.2 Numerical Results

Hereafter we consider the statistical properties of the density fluctuations produced by the texture field. First, we examine the non-Gaussian nature of the source density, $S_x(t,\mathbf{x})$, at each time in terms of the normalized third moment :

$$\Gamma_S(t) \equiv \frac{\langle \Delta S_x(t,\mathbf{x})^3 \rangle}{\langle \Delta S_x(t,\mathbf{x})^2 \rangle^{\frac{3}{2}}} , \tag{4.25}$$

where brackets imply averaging over the spatial configuration. Figure 4.9 shows the time evolution of $\Gamma_S(t)$. It is confirmed that the energy of the texture field has a positively skewed distribution. However, $\Gamma_S(t)$ shows the statistical properties of the source term only at each time slice. By integrating (4.24) to find the matter perturbation, $\delta(t,\mathbf{x})$, we can determine the properties of the observable quantity.

In order to determine the scale-dependence of the statistical properties, let us consider the normalized skewness, $S(V)$, and the normalized kurtosis, $K(V)$:

$$S(V) \equiv \frac{\langle \delta(V)^3 \rangle}{\langle \delta(V)^2 \rangle^2} , \tag{4.26}$$

$$K(V) \equiv \frac{\langle \delta(V)^4 \rangle - 3\langle \delta(V)^2 \rangle^2}{\langle \delta(V)^2 \rangle^3} , \tag{4.27}$$

where $\delta(V)$ is the value of the matter perturbation averaged over the cubic volume V. They are so defined that both quantities should be constant in the hierarchical distribution (4.21). Figure 4.10 and 4.11 show the scale-dependence of $S(V)$ and $K(V)$ at the equality time, when the horizon scale corresponds to $V \simeq 42^3$ in the simulation box. The plotted error is a statistical one which was estimated from 10 different simulations. We can say that the skewness and the kurtosis are nearly constant, $S \simeq 3$ and $K \simeq 15$, within a scale much smaller than the horizon. We performed many simulations in boxes having various physical lengths and this hierarchical behavior has been found to be a general tendency.

In the standard CDM model, the initial distribution of fluctuations is assumed to be Gaussian, and nonlinear evolution produces higher moments of the matter perturbation. The hierarchical behavior of the skewness and kurtosis can be derived from higher order perturbation theory in the matter dominated era[127, 130]. We have shown that the texture model predicts that the hierarchy of the skewness and the kurtosis already exists at the equality time before the onset of mass accretion due to its self-gravity. One can confirm

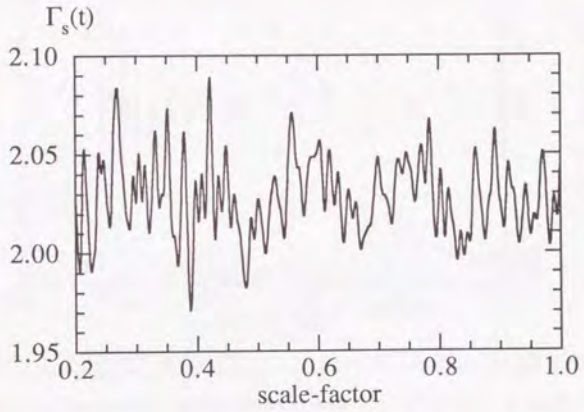

Figure 4.9: Time evolution of $\Gamma_s(t)$ in the 70^3 box. The horizontal axis represents the scale-factor a, with $a = 1$ corresponding to the equality time.

that the observed non-Gaussian nature of the density fluctuations at the equality time is entirely due to the property of texture field, with no effect of nonlinear gravitational interaction, using the second-order perturbation equation[127] :

$$\ddot{\delta}_2 + 2\frac{\dot{a}}{a}\dot{\delta}_2 = 4\pi G(\bar{\rho}_m\delta(1+\delta) + \Delta S_x) - G\bar{\rho}_m\nabla\delta\cdot\nabla\int d^3x'\frac{\delta(x')}{|\mathbf{x}'-\mathbf{x}|} + \frac{1}{a^2}\partial_\alpha\partial_\beta\left(v^\alpha v^\beta\right) , \tag{4.28}$$

$$\mathbf{v} = \frac{a}{4\pi}\frac{\partial}{\partial t}\left(\int d^3x'\delta(x',t)\frac{\mathbf{x}'-\mathbf{x}}{|\mathbf{x}'-\mathbf{x}|}\right) , \tag{4.29}$$

where δ_2 is the amplitude of fluctuation evaluated up to the second order. At the equality time, $a_{eq} = 1$, we measured the amplitude of the four terms of the right-hand side of the equation (4.28) in a 30^3 box. We found that the second term is only 10^{-4} of the first term, and that the third term is 10^{-2} at the scale $\sim$ 1Mpc. We can thus safely say that the second-order effect is much smaller than that of the texture field at the equality time.

However, to show that the effect of non-Gaussian initial fluctuations is significant, they must be compared with the nonlinear effect in the matter-dominated era. We can also

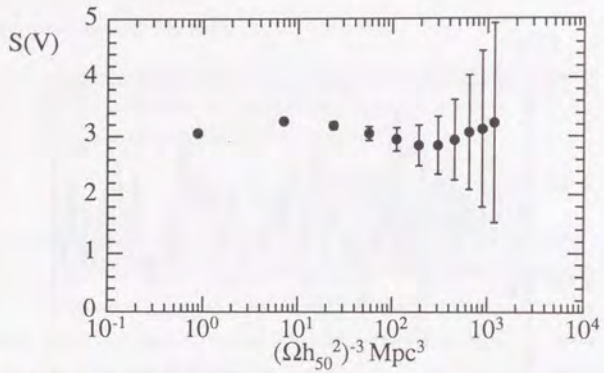

Figure 4.10: Normalized skewness, $S(V)$, as a function of the averaging-volume, V. They are the average of 10 simulations calculated from the spatial distribution of δ in a 100^3 box integrated from $a = 0.2$ to $a = a_{eq} = 1$. The statistical errors are also shown. Ω is the density parameter today and h_{50} is the Hubble constant in units of 50 km s^{-1}Mpc^{-1}. The horizon volume at this time corresponds to $V \sim 40^3(\Omega h_{50}^2)^{-3}\mathrm{Mpc}^3 = 42^3$ meshes in the simulation box. The scale, which contains one knot on the average, is then still 100-times larger than this volume.

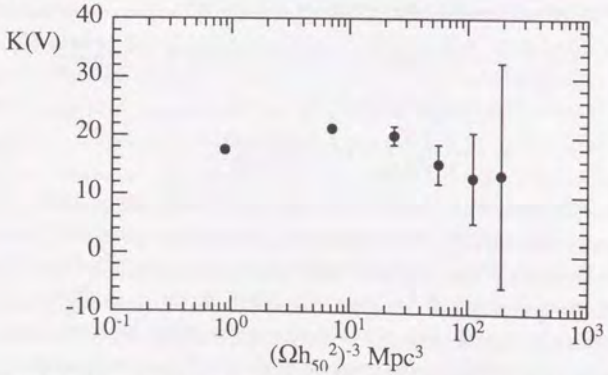

Figure 4.11: Normalized kurtosis, $K(V)$, under the same condition as in Figure 4.10.

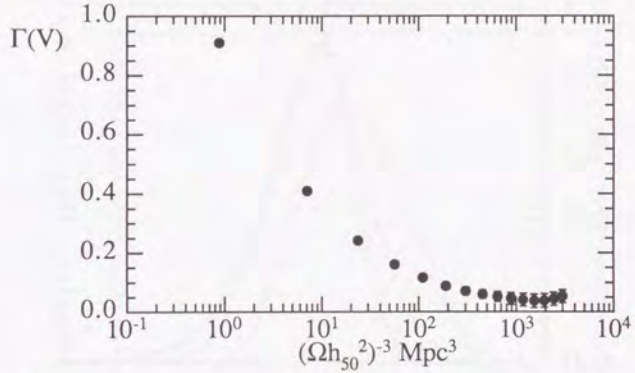

Figure 4.12: Normalized third moment, $\Gamma(V)$, under the same condition as in Figure 4.10.

estimate the effect of the initial skewness and kurtosis to the evolution of fluctuations using the second-order matter perturbation δ_2. The moments of δ_2 are expressed by[132]

$$\langle \delta_2^2 \rangle = \langle \delta^2 \rangle + \langle \delta^3 \rangle , \tag{4.30}$$

$$\langle \delta_2^3 \rangle = \langle \delta^3 \rangle + \frac{34}{21}\langle \delta^4 \rangle , \tag{4.31}$$

$$\langle \delta_2^4 \rangle = \langle \delta^4 \rangle , \tag{4.32}$$

where the moments higher than 5 are neglected. With $\langle \delta^3 \rangle = S\langle \delta^2 \rangle^2 \simeq 3\langle \delta^2 \rangle^2$ and $\langle \delta^4 \rangle - 3\langle \delta^2 \rangle^2 = K\langle \delta^2 \rangle^3 \simeq 15\langle \delta^2 \rangle^3$, the skewness S_2 and the kurtosis K_2 estimated up to the second order are given by

$$S_2 = \frac{S + \frac{34}{7} + \frac{34}{21}K\langle \delta^2 \rangle}{(1 + S\langle \delta^2 \rangle)^2} \simeq 8 , \tag{4.33}$$

$$K_2 = \frac{K - 6S - 3S^2\langle \delta^2 \rangle}{(1 + S\langle \delta^2 \rangle)^3} \simeq -3 , \tag{4.34}$$

respectively. Although the normalized skewness is more enhanced ($S_2 \sim 8$) than in the case of the Gaussian initial condition ($S_2 \sim 5$), the degree of enhancement is not very extreme. As for the normalized kurtosis, $K_2 = 0$ in the initial Gaussian model. The nonzero kurtosis appears in the third-order perturbation and its amplitude is estimated to be ~ 46 by Fry[130]. This is much larger than $|K - 6S| \sim 3$. We thus conclude that even if there exist nonzero higher moments with the hierarchical property, they will be concealed

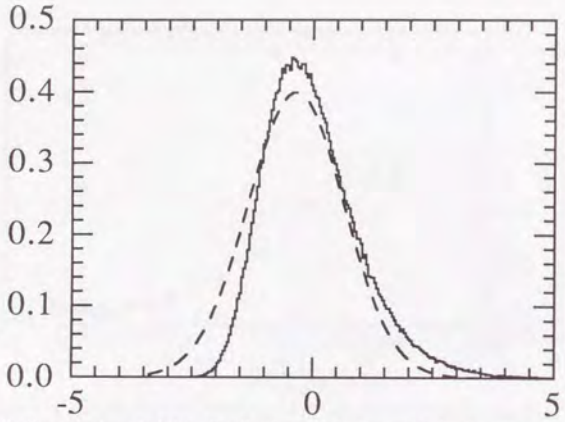

Figure 4.13: Smoothed probability distributions of δ at $a = 1.0$ in the case of a 70^3 box simulation. The averaging-scale is $V = 1^3(\Omega h_{50}^2)^{-3}$ Mpc^3. The horizontal axis is normalized by the variances of δ, which equals 1.5×10^{-6}. The vertical axis is rescaled so that the total area of the distribution is unity. The dashed lines correspond to the Gaussian distribution with the same variance.

by the effect of nonlinear evolution. Since such effect is present in the Gaussian models as well, texture-induced skewness and kurtosis are not necessary for the hierarchical clustering.

In order to estimate how much the non-Gaussian feature is useful for early structure formation, it is important to know to what extent the probability distribution of δ spreads to the side of the high density in the unit of $\langle\delta^2\rangle$. For this purpose, the normalized third moment, $\Gamma(V) \equiv \langle\delta(V)^3\rangle/\langle\delta(V)^2\rangle^{3/2}$, is depicted in Figure 4.12. It drops rapidly before the averaging scale reaches the horizon scale beyond which the field has no correlation. Although the relation $\langle\delta(V)^3\rangle \propto \langle\delta(V)^2\rangle^{3/2}$ is generally expected in non-Gaussian models from an intuitive analysis[133], the third moment of texture-induced fluctuations decreases much more steeply. To see this tendency explicitly, the probability distributions at three different averaging-scales are plotted in Figure 4.13, 4.14 and 4.15. In the scale of $1(\Omega h_{50}^2)^{-1}$Mpc (today shown by Figure 4.13), mass concentrations that have a large deviation from the average to the higher side exist. For example, the portion where δ is larger than three standard deviations (σ_δ) reaches about 1% of the total box volume, while in the Gaussian

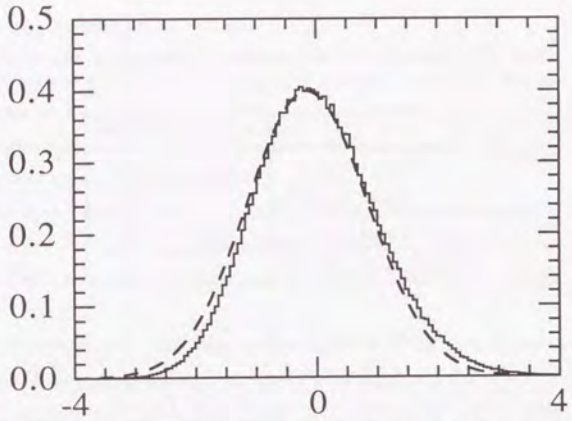

Figure 4.14: The same distribution as Figure 4.13 in the case that the averaging-scale is $V = 3^3(\Omega h_{50}^2)^{-3}$ Mpc^3 and the variance equals 9.7×10^{-8}.

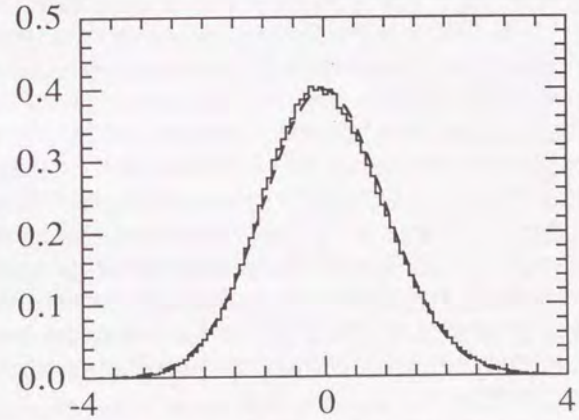

Figure 4.15: The same distribution as Figure 4.13 in the case that the averaging-scale is $V = 6^3(\Omega h_{50}^2)^{-3}$ Mpc^3 and the variance equals 1.6×10^{-8}.

Table 4.1: Percentage of the volume where δ is larger than some $\sigma_\delta(\%)$

	$\delta \geq +2\sigma_\delta$	$\delta \geq +3\sigma_\delta$
Figure 4.13	4.0	0.98
Figure 4.14	3.0	0.29
Figure 4.15	2.8	0.21
Gaussian distribution	2.3	0.13

case it amounts to only 0.13%, as can be seen in Table 4.6.2. This result agrees with the fact that $\Gamma \sim 1$, which can be seen from Figure 4.12. Thus, in the star-formation scale, which is much smaller than $1(\Omega h_{50}^2)^{-1}$Mpc, density peaks of large amplitude can cause quick matter accretion and a prompt shift to non-linear evolution, compared with the Gaussian model. On the other hand, the distribution becomes practically Gaussian at $V \simeq 6^3$, which is much smaller than the mean volume containing one knot. It corresponds to a length scale of $l \simeq 6(\Omega h_{50}^2)^{-1}$Mpc today. Since the texture model does not generate the prominent density peaks in the large-scale structure, the distinction between it and the Gaussian model is practically negligible on galactic scales. This volume dependence comes from a loss of the highly non-Gaussian feature by summing up many small scale fluctuations which are produced by the radial-mode oscillation of the field. Not only the knot unwinding process, but the field oscillation is also indispensable to reproduce the correct statistical properties in the texture model. The importance of the variation in the field amplitude can also be seen from the fact that Pen et al.[122] in which they fixed the field strength $\chi^j\chi^j = v^2$ offered the perturbation which has more power on large scales than that calculated in our simulations. Above results are consistent with the calculation[134] which advocates that linear velocity fields in the large-scale for the non-Gaussian perturbation model are smeared out and look like nearly Gaussian.

4.7 Summary

We have calculated the time evolution of global textures in an expanding universe. The scale-factor has been taken into account precisely. A wide area of the parameter space has been surveyed and the texture evolution shows the scale-invariant behavior in both knot collapses and density peaks distribution.

We have identified topological singularities, *i.e*, the cells in false vacuum as knots. The number of knots per horizon volume is constant. If knots unwind at the speed of light, the rate of knot collapses per comoving density per conformal time interval, $dn_k/d\tau$, is written by

$$\frac{dn_k}{d\tau} = \frac{N_k}{\tau^4}. \tag{4.35}$$

Our simulations show $N_k \sim 0.01$ in the radiation-dominated universe and $N_k \sim 0.02$ in the matter dominated universe. However, knots exhibit only high winding number collapses and the number density of them is not enough to describe all the properties of textures.

The spatial distribution of the gravitational source density, $\rho + 3P$, reveals that the high density peaks are strongly correlated. If a large high density cluster forms a large mass concentration and a small cluster forms a small mass clump, which is a natural assumption, the perturbations by global textures form structures of various sizes within the horizon scale. Moreover, the size distribution profile is constant even in the course of the texture evolution.

These two scale-invariances arise from the property of the dynamical evolution of χ, that is, the continuous phase arranging process. By increasing the horizon, the configuration of the Higgs field comes to be uniform over a larger scale. In particular, not only the Goldstone-mode but also the mass-mode oscillation of the field play an important role in this process. Such fluctuations of the field perturb the metric of the universe on the scales of wide range. Hence global textures generate matter density perturbations in various scales.

However, although the texture model may predict positively skewed non-Gaussian fluctuations on scales relevant to early star formation to reionize the universe, the initial distribution of the perturbations becomes practically Gaussian at $\sim 6(\Omega h_{50}^2)^{-1}$Mpc. The extent of the non-Gaussian feature in this model is at most comparable to that of the hierarchical model. In terms of the normalized skewness and kurtosis, the initial deviation from the Gaussian distribution by textures has less efficiency of matter accretion than does the sub-

sequent nonlinear perturbation growth. We therefore conclude that this model is no better than the standard Gaussian CDM model with regard to the formation epoch of galaxies.

For all that, analyses of the statistical and clustering properties of fluctuations might be useful for comparing the theoretical model with the observed universe. The inflationary model or other topological defects model would be discriminated from the Π_3 nontrivial defects model if we could observe how the primordial fluctuations distribute at or before the equality time. Topological instability of the dynamical evolution causes the distinct features of global textures.

Chapter 5

Conclusion

In this thesis, various aspects of the creation of topological defects during the cosmological phase transitions and the evolution of them in the early universe are reported. Such defects are inevitable products of spontaneous symmetry breakings(SSB) which are the indispensable concept in the unification of elementary interactions. The most successful model in which the SSB plays a central role is the Glashow-Weinberg-Salam theory[135]. It unifies the electromagnetic interaction and the weak interaction, and explains many high energy experiments. Although the Higgs field, a scalar field which causes SSB, has not been found in accelerators on earth, not a little physicists hope that the discovery of it would be a question of time or energy. Even if the Higgs mechanism is wrong, our universe must have experienced some symmetry breaking as long as we believe that the interactions should be consolidated into the sole one in extremely high energy ages. Therefore the topological defects are destined to be recorded on the cosmic chronological table for the most cases..

In the chapter 2, the creation mechanism of topological defects is argued. The conventional scenario is based on the Kibble mechanism in which the thermal correction to the effective potential of the Higgs field causes the symmetry restoration. Although this mechanism is valid only under the thermal equilibrium, the universe might fail to be thermalized in the grand unification era. In the very early universe, the reaction rate of particles is less rapid than the cosmic expansion rate. Thus we have to assume either that the universe started with the thermal equilibrium state as an initial condition or that it was in a chaotic state. As stated in the chapter 2, even in the latter case the production of topological defects is possible in the inflationary universe. The chaotic inflation occurs when the universe

is in a non-equilibrium state and quantum fluctuations push up the field strength so that the effective cosmological constant is acquired. The inflation solves problems which the standard Big Bang model cannot explain. Moreover it can save topological defects from the failure of the production even in a chaotic universe.

In the quantum phase transition mechanism there are two novel problems compared with the original Kibble mechanism. One is that the extended fluctuations by the inflation generate the correlation of the defect field on the scale beyond the Hubble horizon. Hence the distribution of the field value at the time of defect creation differs from the thermal phase transition case. The other problem is related to "the time of defect creation". To determine when the phase transition terminates is not a simple issue. We have considered the dynamical evolution of a scalar field in the chaotic inflationary background. The value of the field can be regarded to be definite when the classical potential force overcomes the random force by quantum fluctuations. From the results of such considerations, we have deduced the spectrum of domain sizes. In contrast to the thermal creation in which only the horizon scale domain exists, various sizes of domains are produced so that various sizes of topological defects come into existence. It is shown that their energy distribution is almost scale-invariant with small- and large-scale cutoffs. Such cutoffs are originated from the causality of the field correlation.

Thus the inflation can be a relief for the Kibble mechanism if it does not dilute the number density of topological defects. We can say that the production of topological defects in the cosmic history is a quite universal phenomenon whether the early universe is chaotic or in equilibrium. After the creation mechanism is investigated, we have payed attention to the evolution of an individual topological defect. At first, in the chapter 3, composite systems of domain walls and cosmic strings are taken up. Such a defect appears in the axion model, which is proposed to give a solution to the strong CP problem. In order to prevent the setback of the standard view of the cosmological evolution, axionic domain walls must be annihilated away otherwise they overclose the universe by their energy density. We have followed the evolution of the axion field and showed that the above catastrophic scenario can be avoided. Moreover, the collapse of a wall-string system is so rapid that enough motion for gravitational radiation does not happen. It indicates that the energy of axionic domain walls is released as field oscillations and another mechanism of axion production is needed

to be considered in detail.

The assertions that axion domain walls disappear efficiently enough or that the domain wall collapse does not provide an experimental constraint by terrestrial gravitational wave observatories are rather passive. As a constructive property of domain walls, we have examined the possibility if they can contribute the large-scale structure formation in the universe. The exact general relativistic solution for the infinite static domain wall shows that the sheet-like false vacuum energy exercises the repulsive force to matter. However, realistic domain walls that appear in cosmological phase transitions must have been moving to a certain degree. Such walls act as attractive sources. Thus the cosmological structure formation scenario by repulsive plates should be rewritten. Domain walls are exotic gravitational seeds of structure formation and provide non-Gaussian fluctuations. This is the most distinctive characteristic to the standard cold dark matter model, which can be confirmed by observations. The recent discovery of the finite amplitude of the cosmic background radiation by COBE had a great impact. It assures us of the properness of our standard cosmological view. The progress of the CMBR observation will supply the information for the determination which model is the most reasonable one. The statistical analysis of the temperature fluctuations on the sky is the most promising evidence of the non-Gaussian initial perturbations.

Another candidate of the non-Gaussian sources of matter perturbations is a global texture. Textures are topologically unstable. They are formed and destroyed continuously during the cosmic evolution and disturb the metric of the universe producing the matter perturbations. The fluctuation spectrum by textures is scale-invariant. From the intuitive analysis, it is demonstrated that the fluctuations by textures obey the non-Gaussian statistics. We have integrated the evolution equation of the texture field and show that it is true. However, the superposition of various scales of fluctuations erases its non-Gaussian property on large-scales. Thus the insufficiency of the fluctuation amplitude on very large-scales in the standard model cannot be compensated by global textures. Anyway they can contribute the prompt star formation which might reheat the content of the universe. Thus global textures may supply the sources for the reionization. The statistical behavior of the texture field is analyzed by the exact formulation of the evolution equation in the expanding universe. The inclusion of the full degree of freedom concerning the field oscillation modes is essential.

The works before us utilized incorrect coding and overestimated the non-Gaussian feature of textures. Thus the prediction concerning the CMBR statistics must be reconsidered.

There are other topological defects that are interesting ingredients of the cosmology. Cosmic strings and magnetic monopoloes are also of cosmological interest. We have studied only domain walls and global textures since they are two extreme examples of topological defects; the smallest dimensional defect by discrete symmetry and the unstable topological defect. Their evolution is traced by solving the non-linear equations in which numerical simulations play an important role. The study of cosmic string evolution is also done by the numerical methods. The progress of electric computers in their power will be very helpful in specifying unknown parts or parameters in the scenarios of topological defects formation and evolution. Observationally the increasing resolution of the CMBR observation will enable us the statistical analysis. Then, as we stated above, the non-Gaussianity by strings and/or textures would be proved or denied. The theoretical calculations of fluctuations in CMBR should be invaluable. Another example of observational evidence of or at least constraint on topological defects is the gravitational radiation from string loops and/or domain walls. Although the establishment of experimental devices for gravitational wave(GW) detection is yet on the way, we will possess a new type of astronomical observatory in the near future. Thus it is terribly important to explore the possibility of GW emission by topological defects. Both observational and theoretical advance will bring glorious knowledge to both particle physics and cosmology.

In cosmological context topological defects have two distinctive meanings. One is that some kinds of them should be found somewhere since the phase transitions accompanied by some spontaneous symmetry breakings must have occurred in the early stage of the cosmic history. The other is that they may assist conventional models in building the variety of cosmological structures. In order to utilize the early universe as a high energy physics laboratory, it is desirable that some evidence of the existence of defects is established. However, even if any observation in future fails to show that topological defects exist, we might have to explain why they are not permitted to be born. In any case, it is interesting and exciting that our attempt to imagine how was the ancient universe, which is a rather metaphysical consideration since the universe can never been created again often contributes to physics as an experimental or observational science.

Acknowledgments

It is my great pleasure to thank my thesis adviser, Professor Katsuhiko Sato for his kind advice, stimulating discussions and continuous encouragement. Thanks are as well due to Professor Jun'ichi Yokoyama, who is a collaborator of parts of the present work, for his invaluable suggestions and useful discussions. I appreciate Professor Yasushi Suto and Masahiro Kawasaki improving the manuscript. I would also like to thank Professor David N. Spergel and Dr. Naoshi Sugiyama for helpful comments. I am grateful to Dr. Shoichi Yamada, Dr. Yuichi Kitada, Dr. Tatsushi Suginohara and other colleagues in theoretical astrophysics and cosmology group at the University of Tokyo, for their assistance in carrying through my graduate life. In particular I am indebted to Mr. Takashi Chiba as well as Mr. Yasuhiko Furihata, who often hearten me with their warm words of comfort.

This research was supported in part by the Japanese Grant in Aid for Science Research Fund of the Ministry of Education, Science and Culture. I acknowledge the support by the Fellowships of the Japan Society for the Promotion of Science for Japanese Junior Scientists.

Numerical calculations presented were executed on the HITAC M-680 at the Computer Center of the University of Tokyo, FACOM M780/10S at the Astronomical Data Analysis Center of National Astronomical Observatory of Japan and SUN SPARC stations at Uji Research Center, Yukawa Institute for Theoretical Physics, Kyoto University.

Bibliography

[1] S. Weinberg, *Gravitation and Cosmology*, (John Wiley & sons, New York, 1972).

[2] E. W. Kolb and M. S. Turner, *The Early Universe*, (Addison-Wesley Publishing Company, Redwood City, 1990).

[3] A. C. S. Readhead, C. R. Lawrence, S. T. Myers, W. L. W. Sargent, H. E. Hardebeck and A. T. Moffet, Ap. J. **346**(1989)566.
T. Gaier, J. Schuster, J. Gundersen, T. Koch, M. Seiffert, P. Meinhold and P. Lubin, Ap. J. **398**(1992)L1.

[4] G. F. Smoot, C. L. Bennett, A. Kogut, E. L. Wright, J. Aymon, N. W. Boggess, E. S. Cheng, G. De. Amici, S. Gulkis, M. G. Hauser, G. Hinshaw, P. D. Jackson, M. Janssen, E. Kaita, T. Kelsall, P. Keegstra, C. Lineweaver, K. Loewenstein, P. Lubin, J. Mather, S. S. Meyer, S. H. Moseley, T. Murdock, L. Rokke, R. F. Silverberg, L. Tenorio, R. Weiss and D. T. Wilkinson, Ap. J. **396**(1992)L1.

[5] J. D. Barrow and F. J. Tipler, *The Anthropic Cosmological Principle*, (Clarendon Press, Oxford, 1986).

[6] K. Sato, Mon. Not. R. astr. Soc. **195**(1981)467.
K. Sato, Phys. Lett. **B99**(1981)66.

[7] D. Kazanas, Ap. J. **241**(1980)L59.
A. H. Guth, Phys. Rev. **D23**(1981)347.

[8] A. D. Linde, Rep. Prog. Phys. **47**(1984)925.
K. A. Olive, Phys. Rep. **190**(1990)307.

A. D. Linde, *Particle Physics and Inflationary Cosmology*, (Harwood, New York, 1990).

[9] P. J. E. Peebles, *Principles of Physical Cosmology*, (Princeton University Press, Princeton, 1993).

[10] J. J. Cowan, F.-K. Thielemann and J. W. Truran, Ap. J. **323**(1987)543.
G. Alcaino, W. Liller and F. Alvarado, Ap. J. **330**(1988)569.
C. P. Deliyannis, P. Demarque and M. H. Pinsonneault, Ap. J. **347**(1988)L73.

[11] M. Rowan-Robinson, *The Cosmological Distance Ladder*, (W. H. Freeman and Company, New York, 1985).

[12] J. Narlikar and H. Arp, Ap. J. **405**(1993)51.

[13] R. M. Wald, Phys. Rev. **D28**(1983)2118.
J. Yokoyama and K. Maeda, Phys. Rev. **D41**(1990)1047.
Y. Kitada and K. Maeda, Phys. Rev. **D45**(1992)1416.
Y. Furihata and K. Sato, Class. Quantum Grav. **10**(1993)1147.

[14] K. Sato, in *Cosmology of the Early Universe*, ed. L. Z. Fang and R. Ruffini (World Scientific, Singapore, 1984)p.165.

[15] M. B. Einhorn and K. Sato, Nucl. Phys. **B180**(1981)385.

[16] A. D. Linde, Phys. Lett. **B108**(1982)389.
A. Albrecht and P. J. Steinhardt, Phys. Rev. Lett. **48** (1982)1220.

[17] S. Coleman and E. Weinberg, Phys. Rev. **D7**(1973)1888.

[18] A. H. Guth and S.-Y. Pi, Phys. Rev. Lett. **49**(1982)1110.

[19] D. La and P. J. Steinhardt, Phys. Rev. Lett. **62**(1989)376.

[20] E. W. Kolb, D. S. Salopek and M. S. Turner, Phys. Rev. **D42**(1990)3925.

[21] P. J. Steinhardt and F. S. Accetta, Phys. Rev. Lett. **64**(1990)2740.
J. García and M. Quirós, Phys. Lett. **B243**(1990)45.
R. Holeman, E. W. Kolb and Y. Wang, Phys. Rev. Lett. **65**(1990)17.

[22] A. D. Linde, Phys. Lett. **B129**(1983)177.

[23] S. W. Hawking, Phys. Lett. **B115**(1982)295.
A. A. Starobinsky, Phys. Lett. **B117**(1982)175.

[24] A. L. Berkin, K. Maeda and J. Yokoyama, Phys. Rev. Lett. **65**(1990)141.

[25] H. Murayama, H. Suzuki, T. Yanagida and J. Yokoyama, Phys. Rev. Lett. **70**(1993)1912.

[26] T. W. B. Kibble, J. Phys. **A9**(1976)1387.

[27] T. W. B. Kibble, Phys. Rep. **67**(1980)183.
A. Vilenkin, Phys. Rep. **121**(1985)263.

[28] Y. B. Zel'dovich, I. Y. Kobzarev and L. B. Okun, JETP**40**(1975)1.

[29] C. T. Hill, D. N. Schramm and J. N. Fry, Comments Nucl. Part. Phys. **19**(1989)25.
J. A. Frieman, C. T. Hill and R. Watkins, Phys. Rev. **D46**(1992)1226.
Z. Lalak and B. A. Ovrut, Phys. Rev. Lett. **71**(1993)951.

[30] T. Vachaspati and A. Achúcarro, Phys. Rev. **D44**(1991)3067.

[31] R. H. Brandenberger and A.-C. Davis, Phys. Lett. **B308**(1993)79.

[32] D. P. Bennett and F. R. Bouchet, Phys. Rev. Lett. **63**(1989)2776.
B. Allen and E. P. S. Shellard, Phys. Rev. Lett. **64**(1990)119.

[33] A. Vilenkin, Phys. Lett. **B107**(1981)47.
C. J. Hogan and M. J. Rees, Nature **311**(1984)109.

[34] A. Vilenkin and T. Vachaspati, Phys. Rev. **D35**(1987)1138.
M. Srednicki and S. Theisen, Phys. Lett. **B189**(1987)397.
R. H. Brandenberger, Nucl. Phys. **293**(1987)812.

[35] A. Vilenkin, Ap. J. **282**(1984)L51.
J. R. Gott III, Ap. J. **288**(1985)422.

[36] F. R. Bouchet, D. P. Bennett and A. Stebbins, Nature **335**(1988)410.
D. P. Bennett, A. Stebbins and F. R. Bouchet, Preprint UCRL-JC-110803.

[37] S. W. Hawking, Phys. Lett. **B231**(1989)237.
R. R. Caldwell and E. Gates, Phys. Rev. **D48**(1993)2581.

[38] J. P. Preskill, Ann. Rev. Nucl. Part. Sci. **34**(1984)461.

[39] G. 't Hoot, Nucl. Phys. **B79**(1974)276.
E. B. Bogomol'nyĭ and M. S. Marinov, Sov. J. Nucl. Phys. **23**(1976)355.
J. P. Preskill, Phys. Rev. Lett. **43**(1979)1365.

[40] N. Turok, Phys. Rev. Lett. **63**(1989)2625.

[41] A. K. Gooding, C. Park, D. N. Spergel, N. Turok and R. Gott III, Ap. J. **393**(1992)42.

[42] R. Y. Cen, J. P. Ostriker, D. N. Spergel and N. Turok, Ap. J. **383** (1991)1.

[43] M. Nagasawa and K. Sato, Int. J. of Mod. Phys. **D1**(1992)427.

[44] M. Hindmarsh and T. W. B. Kibble, **D26**(1982)435.
T. Vachaspati and A. Vilenkin, Phys. Rev. **D35**(1987)1131.

[45] T. W. B. Kibble, G. Lazarides, Q. Shafi, Phys. Rev. **D26**(1982)435.

[46] R. D. Peccei and H. R. Quinn, Phys. Rev. Lett. **38**(1977)1440.

[47] M. Fukugita, F. Takahara, K. Yamashita and Y. Yoshii, Ap. J. **361**(1990)L1.

[48] K. Sato, N. Sugiyama and Y. Yoshii, in Proc. the Sixth Marcel Grossmann Meeting on General Relativity, ed. H. Sato and T. Nakamura (World Scientific, Singapore, 1992)p.43.

[49] K. Sato, in Proc. IUPAP conference *Primordial nucleosynthesis and evolution of early universe*, ed. K. Sato and J. Audouze (Kluwer Academic Publishers, Dordrecht, 1991)p.79.

[50] J. M. Bardeen, P. J. Steinhardt and M. S. Turner, Phys. Rev. **D28**(1983)679.
D. H. Lyth, Phys. Rev. **D31**(1985)1792.

[51] E. Harrison, Phys. Rev. **D1**(1970)2726.
Y. B. Zel'dovich, Mon. Not. R. astr. Soc. **160**(1972)1P.

[52] T. Suginohara, PhD Thesis *Numerical Simulations of Structure Formation of the Universe*, (The University of Tokyo, 1992).

[53] M. Davis, G. Efstathiou, C. S. Frenk and S. D. M. White, Nature **356**(1992)489.

[54] N. Sugiyama and N. Gouda, Prog. Theor. Phys. **88**(1992)803.

[55] V. de Lapparent, M. J. Geller and J. P. Huchra, Ap. J. **302**(1986)L1.

[56] M. J. Geller and J. P. Huchra, Science **246**(1989)897.

[57] T. J. Broadhurst, R. S. Ellis, D. C. Koo and A. S. Szalay, Nature **343**(1990)726.

[58] W. Saunders, C. Frenk, M. Rowan-Robinson, G. Efstathiou, A. Lawrence, N. Kaiser, R. Ellis, J. Crawford, X.-Y. Xia and I. Parry, Nature **349**(1991)32.

[59] P. J. E. Peebles, Ap. J. **315**(1987)L73.
P. J. E. Peebles, Nature **327**(1987)210.

[60] J. D. Barrow and P. Coles, Mon. Not. R. astr. Soc. **244**(1990)188.

[61] A. Ortolan, F. Lucchin and S. Matarrese, Phys. Rev. **D38**(1988)465.
I. Yi, E. T. Vishniac and S. Mineshige, Phys. Rev. **D43**(1991)362.
D. S. Salopek, Phys. Rev. **D45**(1992)1139.

[62] K. Yamamoto, M. Nagasawa, M. Sasaki, H. Suzuki and J. Yokoyama, Phys. Rev. **D46**(1992)4206.

[63] J. Silk and A. Vilenkin, Phys. Rev. Lett. **53**(1984)1700.

[64] P. Coles and J. D. Barrow, Mon. Not. R. astr. Soc. **228**(1987)407.
X. Luo and D. N. Schramm, Phys. Rev. Lett. **71**(1993)1124.
L. Perivolaropoulos, Phys. Rev. **D48**(1993)1530.

[65] L. Doran and R. Jackiw, Phys. Rev. **D9**(1974)3320.
S. Weinberg, Phys. Rev. **D9**(1974)3357.
C. Bernard, Phys. Rev. **D9**(1974)3312.

[66] A. Vilenkin, Phys. Rev. Lett. **46**(1981)1169.

[67] J. Ellis and G. Steigman, Phys. Lett. **B89**(1980)186.

[68] M. D. Pollock, Phys. Lett. **B185**(1987)34.

[69] M. Kawasaki and K. Sato, Phys. Lett. **B189**(1987)23.

[70] J. Yokoyama, Phys. Lett. **B212**(1988)273.
J. Yokoyama, Phys. Rev. Lett. **63**(1989)712.

[71] Q. Shafi and A. Vilenkin, Phys. Rev. **D29**(1984)1870.
L. A. Kofman and A. D. Linde, Nucl. Phys. **B282**(1987)555.

[72] E. T. Vishniac, K. A. Olive and D. Seckel, Nucl. Phys. **B289**(1987)717.

[73] D. Sáez and V. J. Ballester, Phys. Rev. **D42**(1990)3321.

[74] G. M. Shore, Ann. of Phys. **128**(1980)376.
B. Allen, Nucl. Phys. **B226**(1983)228.

[75] M. Nagasawa and J. Yokoyama, Nucl. Phys. **B370**(1992)472.

[76] A. D. Linde and D. H. Lyth, Phys. Lett. **B246**(1990)353.
A. D. Linde, Phys. Lett. **B259**(1991)38.

[77] E. J. Copeland, E. W. Kolb and A. R. Liddle, Phys. Rev. **D42**(1990)2911.

[78] R. Basu, A. H. Guth and A. Vilenkin, Phys. Rev. **D44**(1991)340.

[79] D. H. Lyth, Phys. Lett. **B246**(1990)359.

[80] H. M. Hodges and J. R. Primack, Phys. Rev. **D43**(1991)3155.

[81] A. D. Linde, Mod. Phys. Lett. **A1**(1986)81.

[82] T. S. Bunch and P. C. W. Davies, Proc. R. Soc. Lond. **A360**(1978)117.
A. Vilenkin and L. Ford, Phys. Rev. **D26**(1982)1231.
A. D. Linde, Phys. Lett. **B116**(1982)335.

[83] A. A. Starobinsky, *Current topics in field theory, quantum gravity and strings*, Lecture Notes in Physics 246 (Springer, Berlin, 1986)p.107.

[84] S.-J. Rey, Nucl. Phys. **B284**(1987)706.

[85] M. Sasaki, Y. Nambu and K. Nakao, Nucl. Phys. **B308**(1988)868.

[86] D. S. Salopek, J. R. Bond and J. M. Bardeen, Phys. Rev. **D40**(1989)1753.

[87] W. H. Press, B. P. Flannery, S. A. Teukolsky and W. T. Vetterling, *Numerical Recipes* (Cambridge University Press, Cambridge, 1986).

[88] J. E. Kim, Phys. Rep. **150**(1987)1.

[89] G. 't Hooft, Phys. Rev. Lett. **37**(1976)8.

[90] D. H. Lyth, Phys. Lett. **B275**(1992)279.

[91] F. W. Stecker and Q. Shafi, Phys. Rev. Lett. **50**(1983)928.

[92] T. J. Allen, B. Grinstein and M. B. Wise, Phys. Lett. **B197**(1987)66.

[93] P. Sikivie, Phys. Rev. Lett. **48**(1982)1156.
A. Vilenkin and A. E. Everett, Phys. Rev. Lett. **48**(1982)1867.

[94] B. S. Ryden, W. H. Press and D. N. Spergel, Ap. J. **357**(1990)293.

[95] M. Nagasawa, Phys. Lett. **B318**(1993)53.

[96] E. P. S. Shellard, Nucl. Phys. **B283**(1987)624.

[97] K. J. M. Moriarty, E. Myers and C. Rebbi, Phys. Lett. **B207**(1988)411.
E. P. S. Shellard and P. J. Ruback, Phys. Lett. **B209**(1988)262.

[98] L. M. Widrow, Phys. Rev. **D40**(1989)1002.

[99] C. T. Hill and G. G. Ross, Nucl. Phys. **B311**(1988)253.

[100] M. S. Turner, R. Watkins and L. M. Widrow, Ap. J. **367**(1991)L43.
Y. Nambu, H. Ishihara, N. Gouda and N. Sugiyama, Ap. J. **373**(1991)L35.

[101] H. Kubotani, Prog. Theor. Phys. **87**(1992)387.

[102] A. Massarotti and J. M. Quashnock, Phys. Rev. **D47**(1993)3177.

[103] A. Vilenkin, Phys. Rev. **D23**(1981)852.
J. Ipser and P. Sikivie, Phys. Rev. **D30**(1984)712.

[104] L. M. Widrow, Phys. Rev. **D39**(1989)3571.

[105] S. Veeraraghavan and A. Stebbins, Ap. J. **365**(1990)37.

[106] W. H. Press, B. S. Ryden and D. N. Spergel, Ap. J. **347** (1989)590.

[107] L. Kawano, Phys. Rev. **D41**(1990)1013.

[108] M. C. Huang and P. Sikivie, Phys. Rev. **D32**(1985)1560.

[109] F. Wilczek, Phys. Rev. Lett. **49**(1982)1549.

[110] R. L. Davis, Phys. Rev. **D35**(1987)3705.

[111] R. L. Davis, Phys. Rev. **D36**(1987)997.

[112] C. Park, D. N. Spergel and N. Turok, Ap. J. **372**(1991)L53.

[113] N. Turok and D. N. Spergel, Phys. Rev. Lett. **66**(1991)3093.

[114] A. K. Gooding, D. N. Spergel and N. Turok, Ap. J. **372**(1991)L5.

[115] A. Albrecht and A. Stebbins, Phys. Rev. Lett. **68**(1992)2121.

[116] R. Durrer, M. Heusler, P. Jetzer and N. Straumann, Phys. Lett. **B259**(1991)48.
T. Prokopec, A. Sornborger and R. H. Brandenberger, Phys. Rev. **D45**(1992)1971.

[117] N. Turok and D. N. Spergel, Phys. Rev. Lett. **64**(1990)2736.
D. Nötzold, Phys. Rev. **D43**(1991)R961.
M. Barriola and T. Vachaspati, Phys. Rev. **D43**(1991)1056.

[118] X. Luo, Phys. Lett. **B287**(1992)319.

[119] D. N. Spergel, N. Turok, W. H. Press and B. S. Ryden, Phys. Rev. **D43**(1991)1038.

[120] T. Chiba, N. Sugiyama and Y. Suto, Ap. J. to be published.

[121] D. P. Bennett and S. H. Rhie, Ap. J. **406**(1993)L7.

[122] U.-L. Pen, D. N. Spergel and N. Turok, PUP-TH-1375, Princeton Observatory Preprint 485(1993).

[123] A. Stebbins and S. Veeraraghavan, Phys. Rev. **D48**(1993)2421.

[124] T. Prokopec, Phys. Lett. **B262**(1991)215.

[125] R. A. Leese and T. Prokopec, Phys. Rev. **D44**(1991)3749.

[126] M. Nagasawa, K. Sato and J. Yokoyama, Publ. Astron. Soc. Japan **45**(1993)755.

[127] P. J. E. Peebles, *The Large Scale Structure of the Universe*, (Princeton University Press, Princeton, 1980).

[128] E. Gaztañaga and J. Yokoyama, Ap. J. **403**(1993)450.

[129] M. Davis and P. J. E. Peebles, Ap. J. Suppl. **35**(1977)425.

[130] J. N. Fry, Ap. J. **279**(1984)499.

[131] O. Lahav, M. Itoh, S. Inagaki and Y. Suto, Ap. J. **402**(1993)387.

[132] X. Luo and D. N. Schramm, Ap. J. **408**(1993)33.

[133] R. Juszkiewicz and F. R. Bouchet, in Proc. 2nd *DAEC Workshop Meudon Observatory*, ed. G. Mamon (CNRS, Paris, 1991).

[134] R. J. Scherrer, Ap. J. **390**(1992)330.

[135] F. Halzen and A. D. Martin, *Quarkes & Leptons: An Introductory Cource in Modern Particle Physics*, (John Wiley & sons, New York, 1984).